Geosci. Model Dev., 5, 619–648, 2012
www.geosci-model-dev.net/5/619/2012/
doi:10.5194/gmd-5-619-2012

Geoscientific Model Development

Simulations over South Asia using the Weather Research and Forecasting model with Chemistry (WRF-Chem): chemistry evaluation and initial results

R. Kumar[1], **M. Naja**[1], **G. G. Pfister**[2], **M. C. Barth**[2], **C. Wiedinmyer**[2], **and G. P. Brasseur**[3]

[1]Aryabhatta Research Institute of Observational Sciences, Nainital, 263129, India
[2]Atmospheric Chemistry Division, NCAR, Boulder, CO 80307-3000, USA
[3]Climate Service Center, Helmholtz Zentrum Geesthacht, Hamburg 20146, Germany

Correspondence to: M. Naja (manish@aries.res.in)

Received: 15 December 2011 – Published in Geosci. Model Dev. Discuss.: 3 January 2012
Revised: 17 April 2012 – Accepted: 17 April 2012 – Published: 11 May 2012

Abstract. This study presents annual simulations of tropospheric ozone and related species made for the first time using the WRF-Chem model over South Asia for the year 2008. The model-simulated ozone, CO, and NO_x are evaluated against ground-based, balloon-borne and satellite-borne (TES, OMI and MOPITT) observations. The comparison of model results with surface ozone observations from seven sites and CO and NO_x observations from three sites indicate the model's ability in reproducing seasonal variations of ozone and CO, but show some differences in NO_x. The modeled vertical ozone distribution agrees well with the ozone soundings data from two Indian sites. The vertical distributions of TES ozone and MOPITT CO are generally well reproduced, but the model underestimates TES ozone, OMI tropospheric column NO_2 and MOPITT total column CO retrievals during all the months, except MOPITT retrievals during August–January and OMI retrievals during winter. Largest differences between modeled and satellite-retrieved quantities are found during spring when intense biomass burning activity occurs in this region. The evaluation results indicate large uncertainties in anthropogenic and biomass burning emission estimates, especially for NO_x. The model results indicate clear regional differences in the seasonality of surface ozone over South Asia, with estimated net ozone production during daytime (1130–1530 h) over inland regions of 0–5 ppbv h^{-1} during all seasons and of 0–2 ppbv h^{-1} over marine regions during outflow periods. The model results indicate that ozone production in this region is mostly NO_x-limited. This study shows that WRF-Chem model captures many important features of the observations and gives confidence to using the model for understanding the spatio-temporal variability of ozone over South Asia. However, improvements of South Asian emission inventories and simulations at finer model resolution, especially over the complex Himalayan terrain in northern India, are also essential for accurately simulating ozone in this region.

1 Introduction

The anthropogenic emissions of several key trace gases and aerosols have increased substantially in recent years over Asia due to rapid growth in industrial, transportation, urbanization and agricultural activities (e.g. Akimoto, 2003; Ohara et al., 2007; Tanimoto et al., 2009). Tropical Asia is also a region of high photochemical activity due to strong solar insolation and high amounts of water vapor. The rising emissions and high photochemical activity can potentially enhance the concentrations of several secondary pollutants, such as ozone and secondary organic aerosols, which along with primary pollutants have a wide range of potential consequences for health, vegetation, ecosystems, visibility, radiation budget and atmospheric chemistry. Among different Asian regions, South Asia is the least studied region, although pollutants have been seen to influence the atmospheric composition and radiation budget over the cleaner Indian Ocean (e.g. Lal et al., 1998; Lelieveld et al., 2001; Ramanathan et al., 2001; Lawrence and Lelieveld, 2010) and

pristine Himalayas (e.g. Hegde et al., 2007; Kumar et al., 2010; Marcq et al., 2010; Decesari et al., 2010). Further, strong convection during summer/monsoon is also seen to transport South Asian pollutants to the Mediterranean Sea (e.g. Lawrence et al., 2003; Park et al., 2007). Therefore, it is important to study the spatio-temporal distribution of trace species over this region as well as the impact of South Asian pollutants on the air quality and radiation budget of downwind regions.

Numerous efforts have been made since the early 1990s to conduct in situ measurements of both trace gases (e.g. Lal et al., 2000; Naja and Lal, 2002; Naja et al., 2004; Beig et al., 2007; Reddy et al., 2008) and aerosols (e.g. Sagar et al., 2004; Moorthy et al., 2005; Niranjan et al., 2006; Ramachandran and Rajesh, 2007; Satheesh et al., 2009) over the Indian region. Additionally, an international intensive field campaign called Indian Ocean Experiment (INDOEX) (Lal et al., 1998; Ramanathan et al., 2001; Lelieveld et al., 2001) was conducted to study the export of pollutants from South Asia to the surrounding pristine oceanic environments. Another field campaign called Integrated Campaign for Aerosols, gases and Radiation Budget (ICARB) (Moorthy et al., 2008) was conducted to characterize the physicochemical properties and radiative effects of trace gases and aerosols over the Indian subcontinent. However, these efforts focused largely on the measurements of basic trace gases (ozone, CO, NO_x, lighter non-methane hydrocarbons (NMHCs)) and measurements of other gases and radicals like hydroxyl and peroxy radicals; other oxides of nitrogen and heavier NMHCs are nearly non-existent. In view of the above, an intensive field campaign (Regional Aerosol Warming Experiment – Ganges Valley Aerosol Experiment) (http://www.arm.gov/sites/amf/pgh) with primary focus on aerosols is being carried out over northern India with ARIES, Nainital as a main site. Further, poor spatial coverage and lack of continuous measurements hinder the sufficient understanding of the spatio-temporal distribution of these species over India. The scarcity of measurements makes the application of chemical transport models and satellite observations essential for understanding the distribution of trace species and ozone photochemistry over this region.

A few studies have employed global and regional scale offline models over the South Asian region to simulate the spatio-temporal variabilities in ozone, CO and NO_x over the Indian region (e.g. Kunhikrishnan et al., 2006; Beig and Brasseur, 2006; Roy et al., 2008; Engardt, 2008; Sheel et al., 2010). In this study, a fully coupled, online, regional air quality model known as the "Weather Research and Forecasting model coupled with Chemistry" (WRF-Chem) (Grell et al., 2005) has been employed for the first time to conduct a year-long (2008) simulation over South Asia. The main objective of this study is to evaluate the WRF-Chem model over the South Asian region against observations from multiple platforms and to identify the errors and biases in the model simulations. Model evaluation studies are important to establish the model's credibility for future use, which has not been done so far over the South Asian region. The meteorological fields simulated by the model have been evaluated against observations from ground-based, satellite-borne and balloon-borne instruments and NCEP/NCAR reanalysis fields (Kumar et al., 2012). The evaluation of the meteorological variables, including temperature, dew point temperature, water vapor, zonal and meridional wind components, precipitation, and tropopause pressure and the comparison of the model's meteorological biases and errors against a set of benchmarks revealed that the meteorological fields simulated by the model are of sufficient quality for use in chemical transport modeling.

The evaluation of modeled ozone, carbon monoxide and nitrogen oxides is based on comparison with ground-based, balloon-borne and satellite-based observations over the Indian region. The use of satellite-based measurements for evaluating chemical transport models has become common in the recent years, particularly in regions with limited availability of ground-based observations, as is the case for India (e.g. Pfister et al., 2004; Herron-Thorpe et al., 2010; Sheel et al., 2010). The comparison between satellite retrievals and model simulations has also been used to identify uncertainties in the CO and NO_x emissions estimates (e.g. Allen et al., 2004; Han et al., 2009). Here, model results are evaluated against ozone retrievals from the Tropospheric Emission Spectrometer (TES), CO retrievals from the Measurements of Pollution in the Troposphere (MOPITT) and NO_2 retrievals from the Ozone Monitoring Instrument (OMI) and Global Ozone Monitoring Experiment-2 (GOME-2).

In this paper, the WRF-Chem model configuration used in this study is described in Sect. 2. Different datasets obtained from ground-based and space-borne measurements, methodology used for comparing model results with observations and statistical metrics used to assess the model performance are discussed in Sect. 3. The results from this study are presented in Sect. 4 and are summarized in Sect. 5.

2 The Model description

This study uses the version 3.1.1 of the Weather Research and Forecasting model coupled with Chemistry (WRF-Chem), developed under the collaborative efforts of several research institutes led by NOAA, NCAR and DOE/PNNL (http://ruc.noaa.gov/wrf/WG11/). The model domain is defined on a Mercator projection centered at 25° N, 80° E (see Fig. 1) and covers South Asia at 45 km spatial resolution with 90 grid points in both east-west and north-south directions. The vertical grid in the model is composed of 51 levels from the surface to about 30 km with 10 levels within 1 km above the model surface.

Anthropogenic emissions of CO, NO_x, SO_2, non-methane volatile organic compounds (NMVOC), PM_{10}, $PM_{2.5}$, BC and OC are taken from the Intercontinental

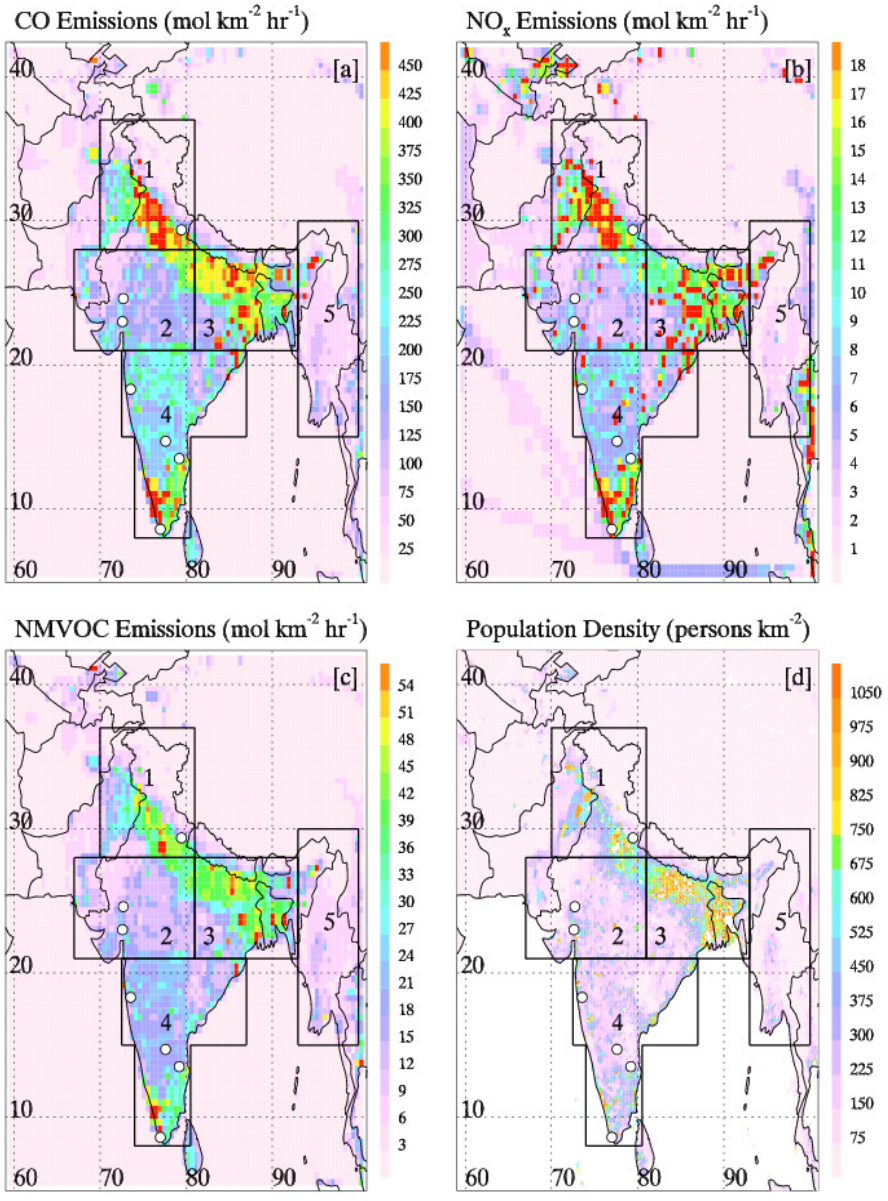

Fig. 1. Spatial distributions of total anthropogenic **(a)** CO, **(b)** NO_x and **(c)** non-methane volatile organic compounds (NMVOC) emissions and **(d)** population density over the simulation domain. The emissions are representative of January. Regional classification of (1) North India, (2) West India, (3) East India, (4) South India and (5) Burma is also shown along with the locations of surface ozone observation sites (white filled circles) over the Indian region.

Chemical Transport Experiment – Phase B (INTEX-B) inventory (Zhang et al., 2009) and the Reanalysis of Tropospheric Chemical Composition (RETRO) (http://retro.enes.org/index.shtml) database. The INTEX-B emissions are representative of the year 2006, and RETRO emissions are representative of the year 2000. The emissions from RETRO are used for the countries west of Pakistan, because the INTEX-B inventory does not provide data over these regions. These emissions data are the most current data available at this time. While we recognize the emissions for 2008 have changed since the compilation of the inventory, no attempt to adjust the emissions has been made. The spatial distributions of the anthropogenic emissions of CO, NO_x and NMVOC over the simulation domain along with that of population density are shown in Fig. 1. The population density is significantly higher over the Indo-Gangetic Plain region followed by Bangladesh and southern parts of India. The distributions of CO, NO_x and NMVOC emissions more or less follow the distribution of population density.

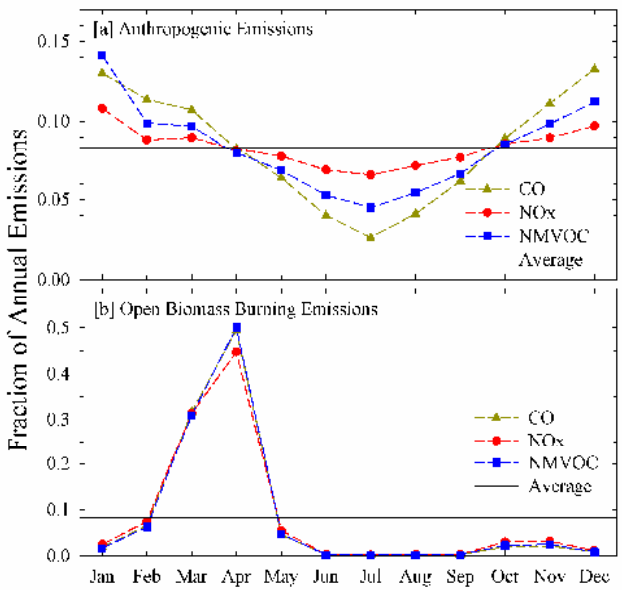

Fig. 2. Seasonal variations in domain-wide **(a)** anthropogenic and **(b)** open biomass burning emissions of CO, NO_x and non-methane volatile organic compounds (NMVOCs) used by the model. The black solid line represents annual average emission.

The percentage contributions of different emissions sectors namely domestic, industry, power and transport sectors to the total annual anthropogenic emissions of major species (CO, NO_x, SO_2, NMVOC, BC, OC and $PM_{2.5}$ and PM_{10}) are shown in Table 1. It is seen that domestic sources (mainly biofuel burning in cooking stoves) are the largest contributors to CO (41 %) and NMVOC (38 %) emissions, while NO_x emissions are dominated by the power (36 %) and transport (34 %) sectors. The larger contribution from domestic sources explains why CO and NMVOC emission sources are spatially more wide-spread, particularly in the rural areas, as compared to the NO_x emission sources. The emissions of particulate matter over the simulation domain are also dominated by the domestic sources.

In addition to the spatial variability, the seasonal variability in anthropogenic emissions over the Asian region has also been suggested to play an important role in air quality simulations (e.g. Han et al., 2009). Since the INTEX-B inventory provides only annual fluxes, the seasonal variation in anthropogenic emissions is extracted from the RETRO inventory and is applied to the annual fluxes from INTEX-B emissions. The estimated seasonal variation is found to be significant only for anthropogenic CO, NO_x and NMVOC emissions (Fig. 2a). The application of a seasonal variation leads to highest anthropogenic emissions during winter and lowest during summer/monsoon.

Daily varying emissions of trace species from biomass burning are provided to the model through the Fire Inventory from NCAR version 1 (FINNv1) (Wiedinmyer et al., 2011). The emissions from FINNv1 are found to agree well with those from Global Fire Emissions Database version 3 (GFEDv3) (Wiedinmyer et al., 2011). The biomass burning emissions are released at the lowest model level. In V3.1.1, the plume-rise biomass emissions parameterization with FINN V1 was not available. The seasonal variations in biomass burning CO, NO_x and NMVOC emissions are shown in Fig. 2b, and the spatial distribution of MODIS-derived fire locations used by FINN is shown in Fig. 3. Biomass burning emissions also exhibit a distinct seasonal cycle with highest values during spring and lowest during summer/monsoon. This is expected because spring is the post-harvesting season, and open crop residue burning is the major practice for clearing agricultural fields in this region (Venkataraman et al., 2006). The total annual biomass burning emissions used by the model for different species are also shown in Table 1. It is seen that total biomass burning emissions are significantly lower than the anthropogenic emissions during all the months except for CO emissions over Burma during February–April. Biogenic emissions of trace species are calculated online using the Model of Emissions of Gases and Aerosols from Nature (MEGAN) (Guenther et al., 2006).

The gas-phase chemistry is represented by the Regional Atmospheric Chemical Mechanism (RACM), which includes 237 reactions among 77 chemical species (Stockwell et al., 1997). The aerosol module is based on the Modal Aerosol Dynamics Model for Europe/Secondary Organic Aerosol Model (MADE/SORGAM) (Ackermann et al., 1998; Schell et al., 2001). The initial and boundary conditions for the chemical fields are updated every 6 h, based on the Model for Ozone and Related Chemical Tracers-version 4 (MOZART-4) results (Emmons et al., 2010). The time step for the chemistry simulation is set to that used for the meteorological simulations, i.e. 180 s, and model results are output every hour. Further details regarding the static geographical fields, initial and lateral boundary conditions for meteorological fields, parameterization of different physical processes, integration schemes and analysis nudging are provided in Kumar et al. (2012) and are not repeated here.

MOZART-4 results are also used here for comparison with WRF-Chem output. The MOZART-4 model is run at about $2.8° \times 2.8°$ horizontal resolution, with 28 vertical levels from the surface to about 2 hPa and is driven by NCEP/NCAR meteorological fields. The model uses anthropogenic emissions from a number of global and regional inventories, biomass burning emissions from Global Fire Emission Database and biogenic emissions from MEGAN. The detailed description of the different emission datasets, model configuration and processes is described by Emmons et al. (2010)

Table 1. Annual total anthropogenic CO, NO_x, SO_2, NMVOC, BC, OC, $PM_{2.5}$ and PM_{10} emissions included in the model. The relative contributions from different source categories to the total emissions over the simulation domain are also listed.

Species	Total annual anthropogenic emissions (Gg)	Percentage contribution from the sector				Total annual biomass Burning emissions (Gg)
		Domestic	Industry	Power	Transport	
CO	76 326	41	30	1	28	26 438
NO_x	6196	6	24	36	34	600
SO_2	9343	9	39	49	3	174
NMVOC	11 962	38	27	2	33	1326
BC	562	59	24	2	15	207
OC	1554	85	10	1	4	409
$PM_{2.5}$	4601	46	36	13	5	546
PM_{10}	5794	38	42	16	4	–

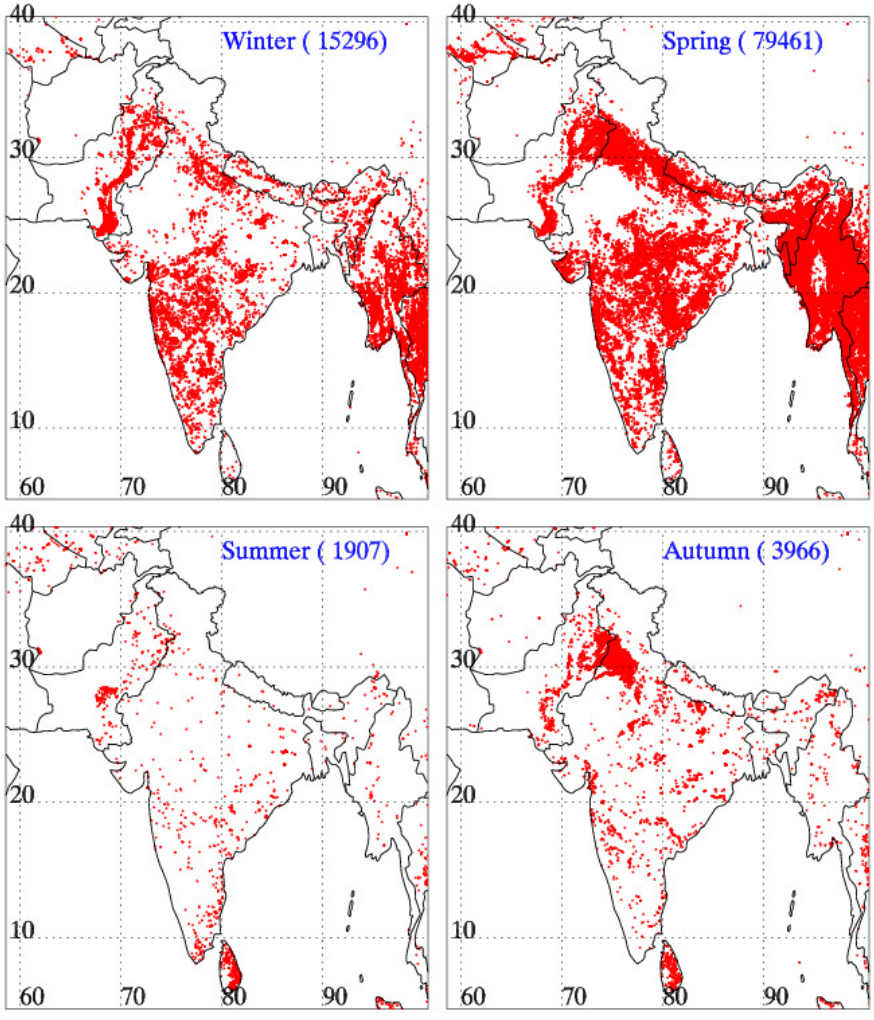

Fig. 3. Spatial distribution of the MODIS-derived fire locations over the model domain during winter (DJF), spring (MAM), summer (JJA) and autumn (SON) of the year 2008. These fire locations are used in FINN for estimating the biomass burning emissions. Numbers in the parenthesis denote total fire counts in each season.

3 Datasets and evaluation methodology

3.1 Ground-based and balloon-borne observations

This study uses surface ozone observations reported from seven sites in India: Ahmedabad (23.0° N, 72.6° E, ∼49 m. a.m.s.l.) (Lal et al., 2000), Gadanki (13.5° N, 79.2° E, ∼375 m. a.m.s.l.) (Naja and Lal, 2002), Mt. Abu (24.6° N, 72.7° E, ∼1680 m. a.m.s.l.) (Naja et al., 2003), Pune (11.7° N, 77.6° E, ∼600 m. a.m.s.l.) (Beig et al., 2007), Anantapur (14.7° N, 77.6° E, ∼331 m. a.m.s.l.) (Reddy et al., 2008), Nainital (29.4° N, 79.5° E, ∼1958 m. a.m.s.l.) (Kumar et al., 2010) and Thumba (8.6° N, 77.0° E, ∼2m amsl) (David and Nair, 2011). The geographic locations of all these sites are shown in Fig. 1 by white filled circles. These sites are representative of different chemical environments, ranging from urban (Ahmedabad), semi-urban (Pune) and rural (Anantapur and Gadanki) to coastal (Thumba) and cleaner high-altitude (Mt-Abu and Nainital) sites. These sites also cover nearly the entire latitudinal extent of India from about 8° N (Thumba) to about 30° N (Nainital). Surface ozone observations at these sites have been made using online ozone analyzers based on the well-known technique of ultraviolet photometry, wwhich is shown to have an absolute accuracy within 5 % (Kleinman et al., 1994). Additionally, surface measurements of CO and NO_x from Ahmedabad, Mt. Abu and Gadanki have been used to evaluate the model simulations. CO observations were made either by analyzing the whole air samples with gas chromatography or by using online CO analyzers based on non-dispersive infrared spectroscopy, while NO_x measurements were made using online analyzers based on the chemiluminescence technique (e.g. Lal et al., 2000; Naja and Lal, 2002; Naja et al., 2003). NO_x values reported in these observational studies could be higher than actual values due to use of molybdenum converters in the analyzers (Steinbacher et al., 2007).

In addition to the surface observations, ozonesonde data in Delhi and Thumba have been obtained for the period 2000–2009 from the World Ozone and Ultraviolet Radiation Data Center (WOUDC) (http://woudc.org/). Ozonesonde data from WOUDC have been used widely for evaluating satellite retrievals (e.g. Worden et al., 2007; Nassar et al., 2008) and model simulations (e.g. Emmons et al., 2010) and to study long-term trends in tropospheric ozone (e.g. Logan, 1994; Cooper et al., 2010). The ozonesonde measurements over India are carried out by the Indian Meteorological Department (IMD) and are based on a modified electrochemical Brewer Bubbler ozone sensor (Shreedharan, 1968), for which the precision is estimated to be better than ±2 % at the peak of the ozone layer (WMO, 1994). These IMD ozonesondes have participated in the Jülich Ozone Sonde Intercomparison Experiment (JOSIE) held in 1996 (Harris et al., 1998). Ozonesonde data from these sites have also been used to study the long-term trends in tropospheric ozone over the Indian region (Saraf and Beig, 2004).

3.2 Satellite-borne observations

This study uses Tropospheric Emission Spectrometer (TES)-retrieved vertical profiles of ozone, Measurement of Pollution in the Troposphere (MOPITT)- retrieved vertical profiles and total column of CO and Ozone Monitoring Instrument (OMI)-retrieved tropospheric column NO_2 abundances. TES aboard NASA's Earth Observing System (EOS)-Aura platform is an infrared Fourier transform spectrometer, which measures the Earth's radiance in the 650–3050 cm^{-1} (15.4–3.3 μm) spectral range with a ground footprint of about 5 km × 8 km in nadir mode (Beer et al., 2001). Aura operates at an altitude of about 705 km in sun-synchronous polar orbit with a local overpass time of about 1345 h±15 min. The radiances measured by TES in the 995–1070 cm^{-1} (10.1–9.3 μm) spectral range are used to retrieve atmospheric ozone concentrations (Bowman et al., 2002; Worden et al., 2004) using an optical estimation approach (Rodgers, 2000). Here, Version 0004 Level 2 TES ozone retrievals from the nominal operational mode (global-survey mode) are used. In the clear sky conditions, TES nadir ozone profiles have approximately 4 degrees of freedom (DFS), two of which generally belong to the troposphere (Bowman et al., 2002; Worden et al., 2004). The vertical resolution of TES nadir ozone profiles as estimated from averaging kernels and error covariances is typically 6–7 km in the troposphere (Worden et al., 2004). The comparison of TES nadir ozone profiles with ozonesonde measurements indicates a positive bias of 3–10 ppbv (Worden et al., 2007; Nassar et al., 2008).

MOPITT aboard the NASA EOS-Terra satellite, flying in a sun-synchronous orbit (local mean solar time of about 1030 in ascending node), is a gas filter radiometer and measures the thermal infrared radiation (near 4.7 μm) with a ground footprint of about 22 km x 22 km. These radiances are then used to retrieve CO mixing ratios profile and total column amounts (Deeter et al., 2003a) using an optimal estimation method (Rodgers, 2000). This study uses version 4.0 Level 2 MOPITT data products, which provide CO mixing ratios at 10 pressure levels between the surface and 100 hPa with a difference of 100 hPa between the levels. The DFS of MOPITT CO retrievals is estimated to be more than 1 over the tropical and midlatitude regions (Deeter et al., 2004). MOPITT CO retrievals have been validated against aircraft CO measurements (Emmons et al., 2004, 2007 and 2009) and are found to be positively biased by about 20 %.

The Ozone Monitoring Instrument (OMI) is also flying aboard NASA's EOS-Aura satellite and measures the radiation backscattered by the Earth's atmosphere and surface over the 0.27–0.5 μm wavelength range with a spatial resolution of about 13 km × 24 km at nadir in normal operational mode. The radiances measured by OMI are used for daily global retrievals of several trace species, such as ozone, NO_2, BrO, SO_2, HCHO and aerosols. Here, we use the tropospheric column NO_2 datasets available from KNMI (Royal Netherlands Meteorological Institute), because it provides

access to the averaging kernel and a priori profiles that play a major role in comparing model results to satellite retrievals (e.g. Emmons et al., 2004). More details on the algorithm used to determine the tropospheric column NO_2 abundances at KNMI are given in Bucsela et al. (2006). The comparison of OMI-retrieved tropospheric column NO_2 amounts at KNMI with INTEX-B aircraft measurements indicates good correlation ($r^2 = 0.67$, slope = 0.99 ± 0.17) between two quantities with no significant biases (Boersma et al., 2008). OMI retrievals are found to correlate well ($r = 0.64$) with MAX-DOAS ground-based measurements (Kramer et al., 2008). However, a number of recent studies have suggested that KNMI OMI retrieval is biased positively, most likely with a magnitude of 0-30 %, irrespective of season (e.g. Boersma et al., 2009a; Zhou et al., 2009).

Level-2 tropospheric column NO_2 retrievals from Global Ozone Monitoring Experiment-2 (GOME-2), derived by KNMI, are also used apart from OMI retrievals. Tropospheric column NO_2 retrievals from GOME-2 are retrieved using essentially the same approach as used for OMI, although some differences exist due to the unique properties of the two instruments (Boersma et al., 2007). The size of the GOME-2 viewing pixel (40 km × 80 km) is also different from OMI (13 km × 24 km). GOME-2 NO_2 retrievals have not been validated directly with in situ observations but are found to compare well with the validated SCIAMACHY retrievals (e.g. Boersma et al., 2009a).

3.3 Evaluation methodology

The model results are compared with ground-based observations by bi-linearly interpolating the model output to the geographical locations of these sites. Unlike in situ observations, satellite retrievals cannot be compared directly with the model output. This is because the retrievals of trace gases from radiances measured by the satellites depend on the relative sensitivity of the retrievals to different altitudes in the atmosphere and on the a priori information about the retrieved trace gas amounts. Thus, any modeled profile must account explicitly for a priori information and sensitivity of retrieved profiles to the true retrievals (as given by the averaging kernel) before its comparison with satellite retrieval.

A two step approach is employed here to compare model results directly with the satellite data. In the first step, best quality satellite retrievals are selected, and the model output is co-located in both space and time with these best quality retrievals. In the second step, the spatially and temporally matched model results are transformed using the averaging kernel and a priori profiles used in the satellite retrievals to obtain a model profile that a satellite instrument would measure for the modeled state of the atmosphere in the absence of other errors. These steps are discussed below.

3.3.1 Data filtering and model satellite co-location

The best quality satellite retrievals are selected by using quality assurance flags and cloud cover information available with each satellite product. TES retrievals are screened for cloudy scenes and unphysical retrievals by selecting the retrievals corresponding to average cloud optical depth of less than 0.1, retrieval quality flag of 1 and O_3 C-cure quality flag of 1 (Osterman et al., 2009). This screening filtered out 55 %, 69 %, 81 % and 67 % of the total TES retrievals during winter (DJF), spring (MAM), summer (JJA) and autumn (SON), respectively. The influence of clouds on OMI retrievals is reduced by selecting pixels with cloud fraction less than 0.3, and unreliable retrievals are removed by selecting pixels with tropospheric column flag equal to 0 (Boersma et al., 2009b). The cloud screening criteria used here are same as those used for generating the level-2G cloud-screened tropospheric NO_2 product from OMI (Celarier, 2009). The screening procedure removed 51 %, 60 %, 68 % and 53 % of total OMI retrievals during winter, spring, summer and autumn, respectively. GOME-2 retrievals are also filtered by selecting pixels with cloud fractions less than 0.3 and tropospheric column flag equal to 0. Further, nighttime pixels from OMI and GOME-2 data are also removed from the analysis. The number of samples accepted for TES, OMI and GOME-2 is lowest during summer because of the prevalence of cloudy conditions over the simulation domain. Unlike TES and OMI, MOPITT retrievals are performed only for cloud-free pixels. MOPITT retrievals were screened for pixels with DFS value greater than or equal to 1. The DFS condition removed 21 %, 11 %, 14 % and 17 % of total MOPITT retrievals during winter, spring, summer and autumn, respectively. The best quality retrievals are then co-located in space and time with model output using the method described in Kumar et al.(2012).

3.3.2 Averaging kernels and a priori profiles

This section describes the procedures used for transforming modeled ozone, CO and NO_2 profiles for direct comparison with TES, MOPITT and OMI retrievals. The model data co-located with the best quality satellite retrievals are first mapped onto the pressure grids of the different sensors. The model top is located at 10 hPa, while the TES pressure grid extends up to 0.1 hPa; therefore, modeled ozone profiles above 10 hPa are approximated by appending the TES a priori profile. The appended modeled profile is then interpolated to a fine level pressure grid (800 levels from 1260 hPa to 0.046 hPa), and then a mapping matrix is used to interpolate the fine level modeled profile to the 67 pressure level TES grid following Worden et al. (2007). The TES averaging kernel A_{TES} and a priori constraint vector $X_{apriori}$ are then applied to the WRF-Chem ozone profile X_{int} (which is now on TES pressure grid) to obtain the WRF-Chem ozone profile WRF-Chem (AK) through the following equation:

$$\text{WRF-Chem(AK)} = X_{\text{apriori}} + A_{\text{TES}}[X_{\text{int}} - X_{\text{apriori}}]. \quad (1)$$

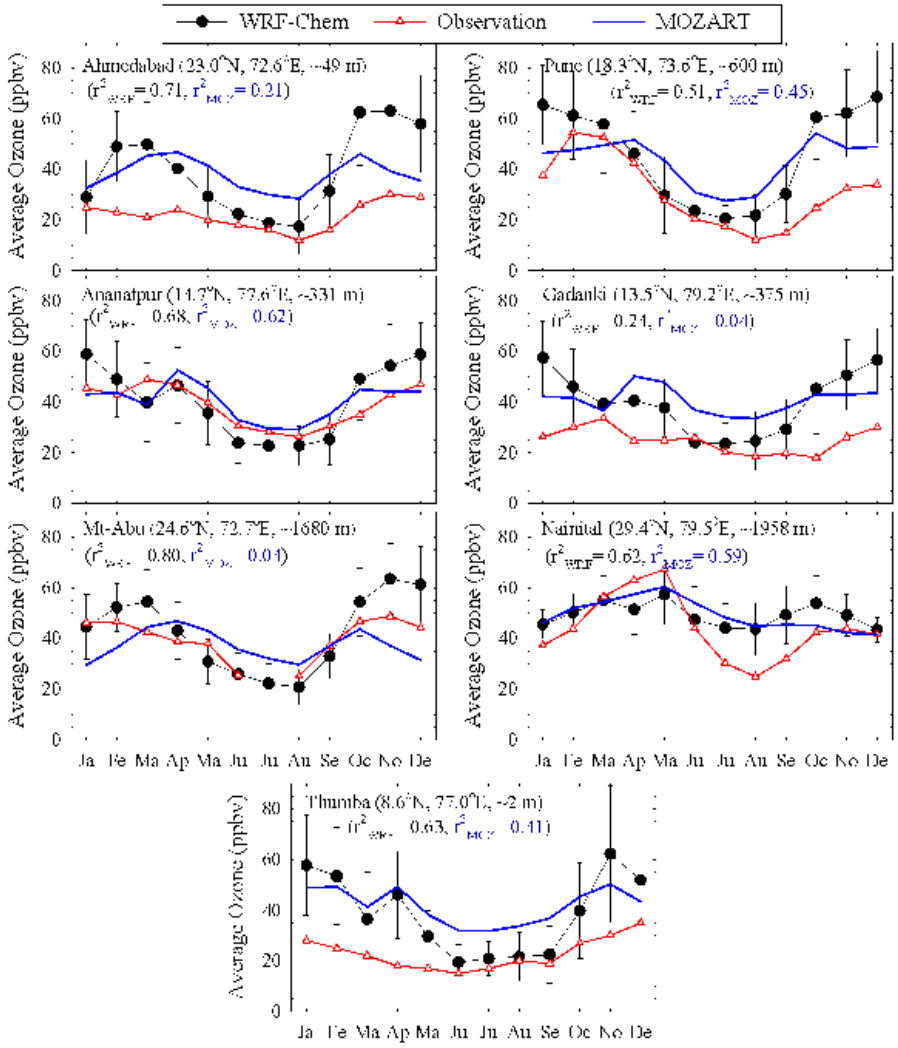

Fig. 4. Comparison of the observed and WRF-Chem simulated seasonal variations in surface ozone at seven sites located within the Indian region. Note that, except for Nainital, the observations are not representative of the year 2008. These sites are representative of urban (Ahmedabad), semi-urban (Pune), rural (Anantapur and Gadanki), coastal (Thumba) and high-altitude cleaner (Mt-Abu and Nainital) chemical environments, respectively. The standard deviations in monthly average ozone levels at these sites are generally 5–20 ppbv, depending upon the season. r^2_{WRF} and r^2_{MOZ} represent the correlation coefficient of WRF-Chem and MOZART with observations, respectively.

The WRF-Chem (AK) accounts for TES sensitivity and vertical resolution. A similar procedure is used to transform the modeled CO profiles using MOPITT averaging kernels and a priori profiles. However, a simple linear interpolation is used to interpolate the modeled profile on to the ten pressure level MOPITT grid from 1000 hPa to 100 hPa (Deeter et al., 2003b).

The procedure for transforming the WRF-Chem simulated tropospheric column NO_2 abundances for comparison to OMI and GOME-2 retrievals is different from that used for TES and MOPITT. This procedure requires the user to calculate the tropospheric averaging kernels (A_{trop}) through the following equation:

$$A_{\mathrm{trop}} = A \cdot \frac{\mathrm{AMF}}{\mathrm{AMF}_{\mathrm{trop}}} \tag{2}$$

where A is the total column averaging kernel and AMF and $\mathrm{AMF}_{\mathrm{trop}}$ are the air mass factors for the total columns and tropospheric columns, respectively. The tropospheric averaging kernels are then applied to the tropospheric vertical profiles of NO_2, simulated by WRF-Chem using the following equation:

$$Y_{\mathrm{trop}} = A_{\mathrm{trop}} \cdot X_{\mathrm{trop}} \tag{3}$$

where Y_{trop} is the transformed model profile and X_{trop} is the tropospheric WRF-Chem NO_2 profile interpolated to the OMI/GOME-2 pressure grid. The tropopause pressure used for estimating tropospheric WRF-Chem profiles is taken from the OMI/GOME-2 data.

3.4 Statistical metrics

Five statistical metrics, namely index of agreement (d), root-mean-square error (RMSE), mean normalized gross error (MNGE), mean bias (MB) and mean normalized bias (MNB) are used to assess the model performance. These metrics were developed by Yu et al. (2005) and have been successfully used in several studies for evaluating the performance of regional air quality models (e.g. Zhang et al., 2006; Han et al., 2009). The index of agreement determines the model skill in simulating the variations around the observed mean and is a dimensionless quantity that varies between 0 (no agreement between model and observations) and 1 (perfect agreement). The MB provides the information about the absolute bias of the model, with negative values indicating underestimation and positive values indicating overestimation by the model. The MNB represents the model bias relative to observations, and RMSE considers error compensation due to opposite sign differences and encapsulates the average error produced by the model. The MNGE represents mean absolute difference between model and observations relative to the observations. The mathematical definition of all these statistical metrics is provided in the auxiliary material.

4 Results of model evaluation

4.1 Ground-based and ozonesonde observations

This section presents the comparison of WRF-Chem simulated ozone, CO and NO_x with ground-based and balloon-borne observations available over the Indian region. Since some of the ground-based observations are available for 1993–2000, while other data are representative of 2000–2010, published data are used here to demonstrate the model's skill in simulating the seasonal variations of these species. The monthly average modeled surface ozone is compared against ground-based observations (Fig. 4), and it is seen that the seasonal variation in surface ozone over India is simulated reasonably well by the model with coefficient of determination (r^2_{WRF}) values in the range of 0.24–0.80.

At some sites, surface ozone is lowest during summer and higher during other seasons. Ozone levels at all the sites, except Nainital, peak between late autumn and early spring, while ozone levels are highest during April–May with a secondary peak during October–November at Nainital. Surface ozone in Pune (in south west India) shows a clear maximum in late winter and early spring, while the two sites in western India (Ahmedabad and Mt Abu) show maximum ozone in late autumn and early winter. This indicates regional differences in the ozone seasonality over the Indian region. The regional differences in ozone seasonality will be explored further using TES retrievals in the next section.

Lower ozone levels observed over the Indian region during summer are in sharp contrast with the seasonal patterns observed typically in North America and Europe (e.g. Logan, 1985; Solberg et al., 2008), but are similar to those observed over East Asia (e.g. Pochanart et al., 2003; Wang et al., 2006). These lower summertime ozone levels over India (e.g. Lal et al., 2000; Naja and Lal 2002; Jain et al., 2005; Roy et al., 2008; Kumar et al., 2010) can be attributed mainly to long-range transport of ozone-poor marine air masses from the Arabian Sea, Indian Ocean and Bay of Bengal with some contributions from reduced photochemical production and wet scavenging of ozone precursors. WRF-Chem ozone levels show significant reduction during summertime at all the sites except at Nainital, and it is seen that these reduced values are in good agreement with the observed values at these sites (Fig. 4). An earlier study employing an offline regional model with comparable spatial resolution showed an overestimation of ozone levels during summer over India (Roy et al., 2008).

Nainital is located in the Himalayan region, where topography is highly complex and the height of mountaintops changes by about 2000 m over a distance of less than 50 km. Therefore, the model resolution of 45 km is unable to resolve the meteorological features induced by rapidly varying topography around Nainital. To assess the impact of the model resolution, we performed a nested domain run for 10 days during 10–20 July 2008. The selection of this period has been motivated by back trajectory analysis (not shown), which revealed consistent influence of marine air masses at Nainital during this period. The nested domain covers the northern Indian region with 121×115 grid points and has a spatial resolution of 15 km (see auxiliary material, Fig. S1). The model-simulated surface ozone from the nested domain is found to agree very well with surface ozone observations in Nainital (see auxiliary material, Fig. S2), as mean bias reduced from 17 ppbv, in the base run, to 3 ppbv in the nested domain model run. This suggests that errors in surface ozone simulations over the central Himalayan region during summer/monsoon can be reduced by employing the model at a higher spatial resolution. However, longer simulations are required for lending more confidence to this finding. A high resolution annual simulation could not be performed for this study due to limited computational resources and because there is not an emissions inventory available at high resolution.

The seasonal variations of MOZART-simulated surface ozone at these sites are also shown in Fig. 4 along with coefficient of determination (r^2_{MOZ}). The ozone seasonality is reproduced well by MOZART at some sites, with coefficient of determination (r^2_{MOZ}) values between 0.41 and 0.62. However, summertime lower ozone levels and ozone

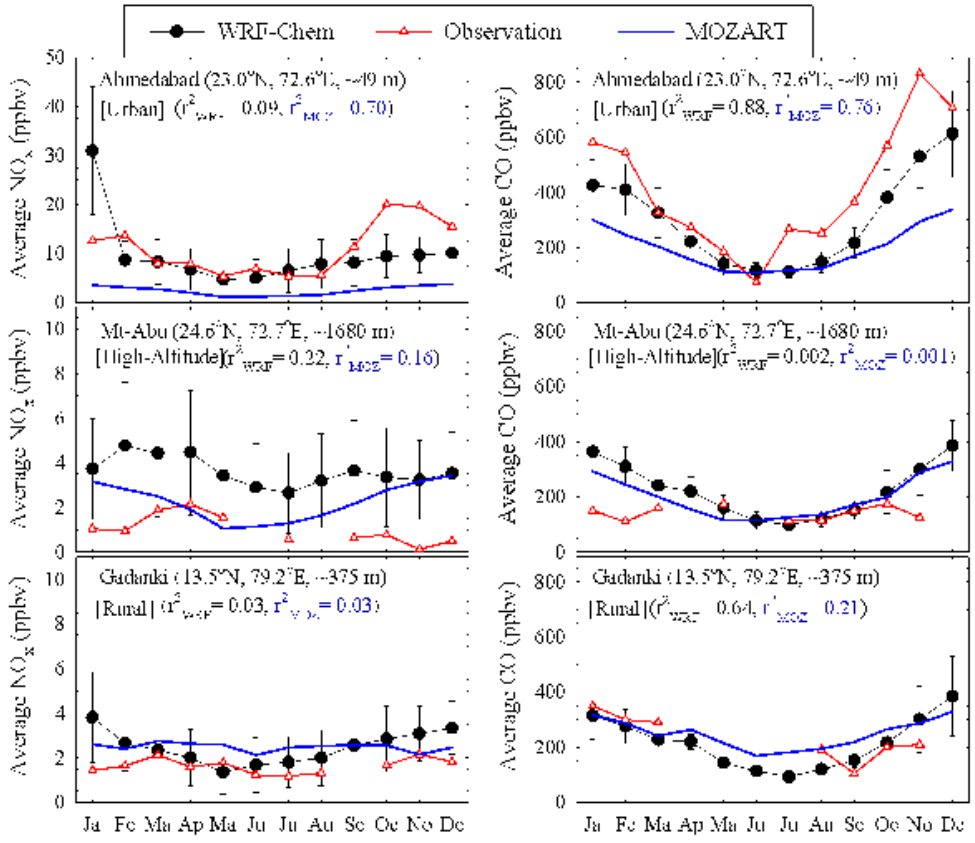

Fig. 5. Comparison of the observed and WRF-Chem simulated seasonal variations in average surface NO_X (left panel) and CO (right panel) at three sites located within the Indian region. Note the scales vary among the sites and that the observations are not representative of the year 2008. The standard deviations in monthly average CO levels at these sites are generally 50–200 ppbv and those in NO_X levels are generally 1–6 ppbv. r^2_{WRF} and r^2_{MOZ} represent the correlation coefficient of WRF-Chem and MOZART with observations, respectively.

variations from September–December are reproduced better in WRF-Chem than in MOZART, as indicated by higher r^2_{WRF}(0.24–0.80) values than r^2_{MOZ} values (0.04–0.62) at all the sites. This is likely due to the coarse horizontal resolution ($2.8° \times 2.8°$) of MOZART. At the global model resolution, the model has limited ability in simulating cloud cover and underestimation of cloud cover will enhance the photochemical ozone production. Transport and dilution errors will also impact the model ozone.

The seasonal variations in near surface monthly average CO and NO_X observed at sites Ahmedabad, Mt. Abu and Gadanki are also compared to those simulated by WRF-Chem and MOZART (Fig. 5). The seasonal variation of CO is reproduced well by the model for all three sites with highest values during late autumn – winter and lowest during summer/monsoon. NO_X values in Ahmedabad are unusually high in January and are due to significantly higher anthropogenic NO_X emissions over Ahmedabad in January ($\sim$120 mol km^{-2} h^{-1}) as compared to other months (20–30 mol km^{-2} h^{-1}). Discrepancies between the observed and modeled NO_X seasonalities are evident at all the sites. The reasons for larger discrepancies in the NO_X results will be discussed in more detail in Sect. 4.2. The seasonal variations in MOZART CO and NO_X values are similar to WRF-Chem except for NO_X variations at Mt.-Abu. Interestingly, MOZART CO values in Ahmedabad (urban site) are found to be lower than WRF-Chem values, while they are similar to WRF-Chem at Mt. Abu (high altitude site) and Gadanki (rural site), which likely is due to the coarser resolution of MOZART-4. Previous studies (e.g. Tie at al., 2010) showed that models at finer resolution capture more local features around urban emission sources, while coarser resolution models tend to dilute concentrations from localized emission sources. The values of r^2_{WRF} are higher than those for r^2_{MOZ} in case of CO but are similar for NO_X, except in Ahmedabad where r^2_{WRF}(0.09) is significantly lower than r^2_{MOZ}(0.7), which is found to be due to unusually higher WRF-Chem values in Ahmedabad in January.

In addition to the ground-based observations, the vertical distribution of the model-simulated ozone in Delhi and Trivandrum is also compared with a 10-yr(2000–2009) climatology derived from ozonesonde observations. The

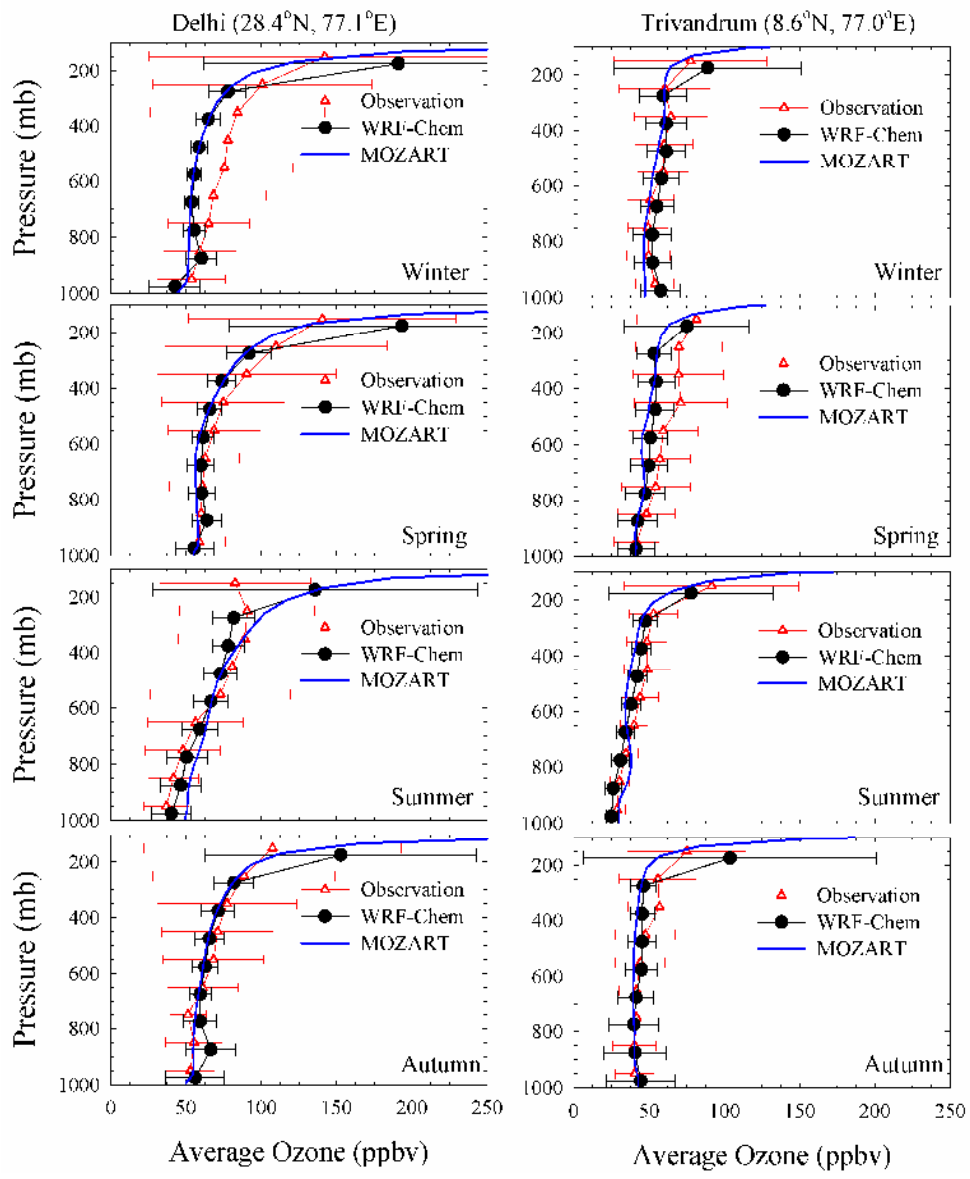

Fig. 6. Comparison of the vertical profiles of ozone mixing ratios observed by ozonesondes and simulated by WRF-Chem in Delhi and Trivandrum. The observed profiles shown here are averages of all the ozonesonde measurements available during 2000–2009. Seasonally averaged MOZART ozone profiles for both sites are also shown to demonstrate the influence of boundary conditions.

comparison for winter, spring, summer and autumn is depicted in Fig. 6. The total number of ozonesonde profiles used to obtain the climatology for Delhi and Trivandrum are 104 and 103, respectively. Both the ozonesonde and model data are averaged over 100 hPa pressure intervals. The vertical gradient as well as the seasonal variability of tropospheric ozone at both the sites are reproduced well by the model, with average modeled values falling within one standard deviation of the climatological mean value below 200 hPa. However, the model underestimates the observed ozone values in the middle and upper troposphere in winter and slightly in spring over Delhi. MOZART ozone values also fall within one standard deviation (Fig. 6) of the climatological mean value and show vertical gradient and seasonal variability similar to WRF-Chem.

4.2 Space-borne observations

The comparison of model-simulated ozone, CO and NO_x against in situ observations presented in the previous section indicates that the model qualitatively reproduces the observed features of lower tropospheric ozone and CO seasonality, but shows discrepancies in simulating NO_x seasonal

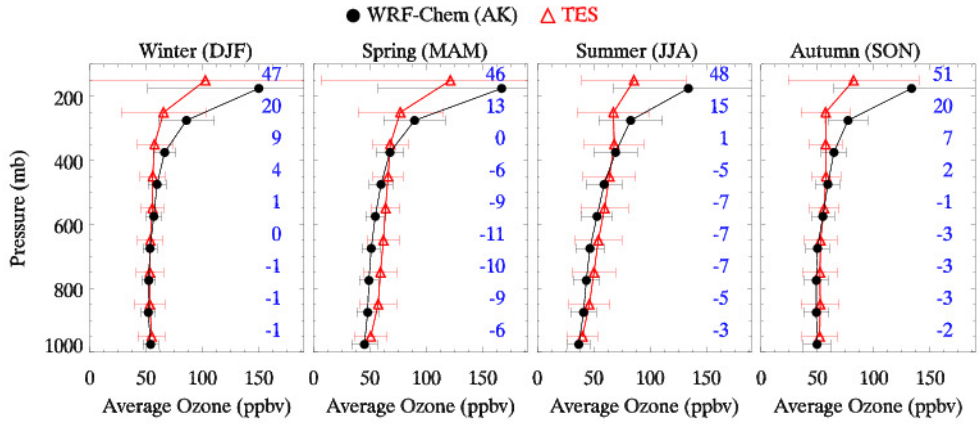

Fig. 7. Comparison of the vertical profiles of ozone mixing ratios retrieved by TES and simulated by WRF-Chem during winter, spring, summer and autumn 2008. WRF-Chem profiles are transformed using TES averaging kernel and a priori profile before this comparison. The vertical profiles are obtained using co-located WRF-Chem and TES data. Numbers on the right in each panel give the difference in ozone mixing ratios between WRF-Chem and TES (WRF-Chem – TES).

variations. However, the model bias and errors were not quantified mainly due to differences in the time periods of observations and model simulations. Further, the comparison was limited to a few sites and thus information about the model performance over larger spatial scales was not obtained. In this section, satellite observations of ozone, CO and NO_2 are used to assess the model performance over the entire domain and to quantify the errors and biases in model simulations. The possible sources of uncertainties in the model simulations are also discussed.

4.2.1 Comparison with TES ozone retrievals

The vertical profiles of model-simulated and TES-retrieved ozone during winter (DJF), spring (MAM), summer (JJA) and autumn (SON) 2008 are shown in Fig. 7. Both the model and TES values are averaged over 100 hPa pressure intervals. Similar to the comparison with ozonesonde observations, the vertical gradients and the seasonal variability of TES-retrieved ozone profiles are reproduced well by the model. The model generally agrees well with TES retrievals below 300 hPa, but overestimates TES ozone above 300 hPa. The absolute difference between average modeled and TES-retrieved values below 300 hPa is less than 12 ppbv during all the seasons, which is comparable to the positive bias of 3–12 ppbv reported in TES retrievals against ozonesonde observations (e.g. Nassar et al., 2008). The difference between WRF-Chem and TES values increases to 10–50 ppbv above 300 hPa. Larger differences between WRF-Chem and TES in the upper troposphere could be due to errors in ozone inflow from domain boundaries, as comparison of TES retrievals with MOZART output within $\pm 10^{\circ}$ longitudinal and latitudinal bands around the domain boundaries revealed that MOZART ozone levels are higher by 10–70 ppbv than TES retrievals above 300 hPa.

Table 2. Seasonal variation in index of agreement (d), mean bias (MB), mean normalized bias (MNB), root-mean-square error (RMSE) and mean normalized gross error (MNGE) computed using the co-located WRF-Chem and TES ozone values (year 2008) in the lower troposphere (Surface – 500 hPa). The total number of data points (N) used in the calculation is also listed.

Month	d	MB[1]	MNB[2]	RMSE[1]	MNGE[2]	N
Jan	0.64	0	3	10	14	4103
Feb	0.65	−1	1	10	15	4020
Mar	0.76	−5	−6	12	16	2919
Apr	0.75	−10	−15	15	18	3007
May	0.68	−11	−16	16	20	2351
Jun	0.76	−10	−14	17	18	1111
Jul	0.81	−7	−8	14	17	1412
Aug	0.90	−3	−1	11	17	2082
Sep	0.88	−3	−2	10	16	3068
Oct	0.83	−2	−1	10	14	3575
Nov	0.75	−2	0	11	15	2668
Dec	0.67	−1	2	10	15	3134

[1] Unit: ppbv
[2] Unit: %

The monthly statistical analysis of TES-retrieved and model-simulated lower tropospheric (surface to 500 hPa) ozone is shown in Table 2. The upper limit of 500 hPa, used in the comparison, is similar to that used in validation studies of TES ozone retrievals (Worden et al., 2007; Nassar et al., 2008) and ensures that TES retrievals have sufficient sensitivity in the comparison region. Worden et al. (2007) showed that TES averaging kernel rows grow, corresponding to pressure values between the surface and 500 hPa peak around 600–700 hPa, indicating that TES has good sensitivity in this region. The index of agreement between model and TES

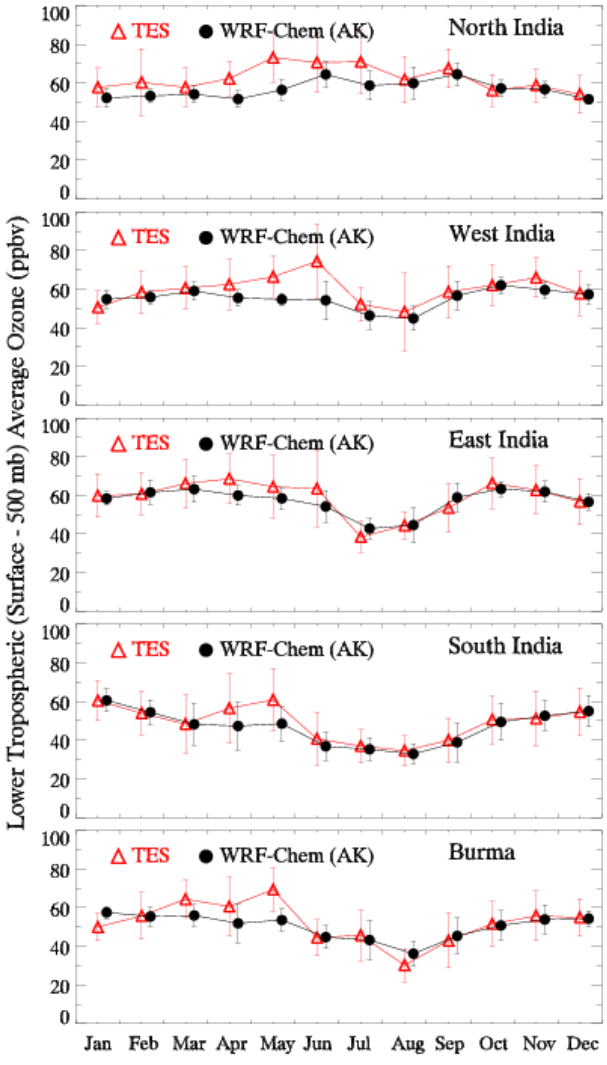

Fig. 8. Seasonal variations in WRF-Chem simulated and TES- retrieved ozone in the lower troposphere (surface-500 hPa) over the five regions defined in Fig. 1.

varies between 0.64 and 0.9 during different months, which indicates good model performance in simulating the observed variation around the TES-retrieved mean value. The model systematically underestimates the TES retrievals leading MB values, ranging from 0 to −11 ppbv during all the months. The MB is smallest from August–February (−1 to −3 ppbv). MNB, RMSE and MNGE also show similar temporal variations, and the estimated range is 0 to −16 %, 10–17 ppbv and 14 % to 20 %, respectively. Larger differences during spring and early summer could be indicative of additional ozone precursor sources (e.g. biomass burning) and chemical processes during this period.

TES retrievals are also used to examine the regional variability in the lower tropospheric ozone over the Indian region and to investigate whether the model is capable of capturing the spatio-temporal heterogeneity. In this context, the seasonal variation of model-simulated lower tropospheric (surface to 500 hPa) ozone is compared with the co-located TES retrievals over four geographical regions of India: North India (28° N–37° N, 70° E–81° E), West India (21° N–28° N, 67° E–81° E), East India (21° N–28° N, 81° E–93° E) and South India (15° N–21° N, 72.5° E–87° E and 8° N–15° N, 74° E–80.5° E) (Fig. 1). The seasonal variation is also examined for the geographical region of Burma, including some part of East India (15° N–30° N, 93° E–100° E), which is characterized by lower anthropogenic emissions and very high fire activity especially during winter and spring (Fig. 3). The comparison over Burma is intended to provide better insight into the model's response to emissions from biomass burning.

The seasonal variations in TES retrievals are captured well by the model except in spring over five regions (Fig. 8), when modeled ozone levels are somewhat lower. Regional differences in seasonality are also evident. Except for North India, ozone is lowest during summer monsoon season, which as previously mentioned is associated mainly with the prevalence of long-range transport from clean, marine air masses coupled with cloudy conditions and extensive rainfall due to monsoonal circulation. For North India we find highest ozone during spring–summer and lowest values during winter. The spring to summer decrease in ozone values is observed during June over South India and Burma, and in July over West and East India.

To understand the regional differences in ozone seasonality over these regions, model-simulated 2 m height water vapor mixing ratios and surface-reaching daytime (07:30–17:30 IST; IST is 5.5 h ahead of GMT) solar radiation are analyzed. The water vapor mixing ratios are found to be highest during summer/monsoon over all the regions, but their values are significantly smaller over North India (2–11 g kg^{-1})than those over other regions(4–21 g kg^{-1}) (Auxiliary material, Fig. S3a). Like ozone, the seasonal variations in solar radiation over North India are also different from the other regions, with highest values in spring–summer (Auxiliary material, Fig. S3b). This suggests that regional differences in ozone seasonality over India are associated with temporal differences in the start of the monsoon and the arrival of pristine marine air masses to the respective regions. Such latitudinal differences in transition from spring maximum to summer minimum have also been reported over East Asia and associated with the spatially varying influence of Asian monsoon (e.g. He et al., 2008; Lin et al., 2009).

Another notable regional difference is observed during the transition from autumn to winter season. TES ozone over South India continues to increase from summer through autumn–winter, while ozone over other regions increases from summer–autumn and decreases or becomes steady during winter. This is due to the availability of higher solar radiation over South India as compared to other regions during winter (Auxiliary material, Fig. S3b). The differences

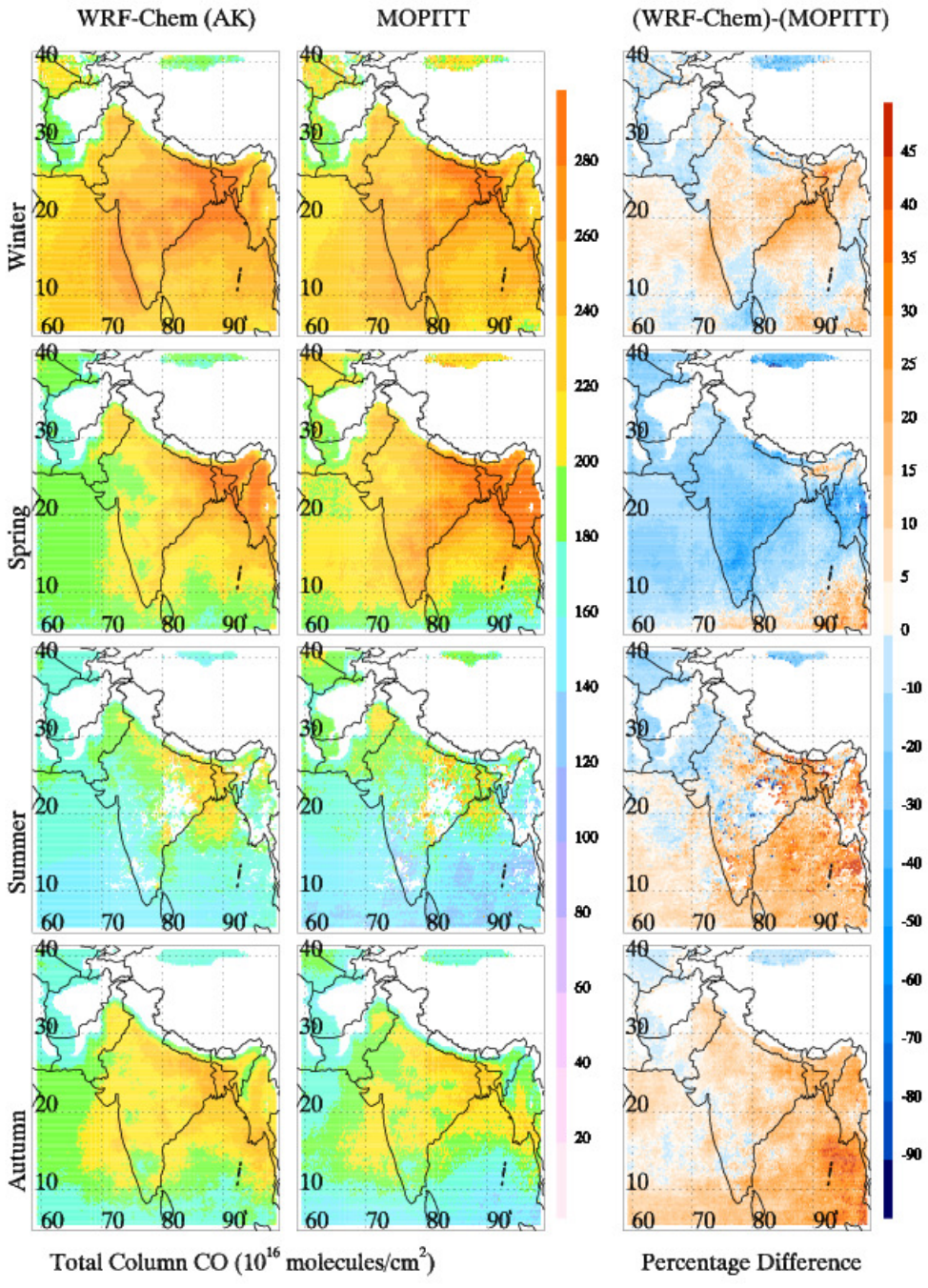

Fig. 9. Spatial distributions of WRF-Chem simulated and MOPITT- retrieved total column CO during winter (DJF), spring (MAM), summer (JJA) and autumn (SON) 2008. Note that WRF-Chem profiles are smoothed with MOPITT averaging kernel before comparison.

between TES and WRF-Chem are largest during spring and particularly over North India. The poor agreement between the model and TES over North India is likely associated with improper representation of surface properties and errors in meteorological simulations due to complex topography over this region (Kumar et al., 2012). The errors in model- simulated ozone during spring could also result, in part, due to underestimation of CO and NO_x by the model (likely due to underestimation of CO and NO_x emissions by biomass burning), as shown in subsequent sections.

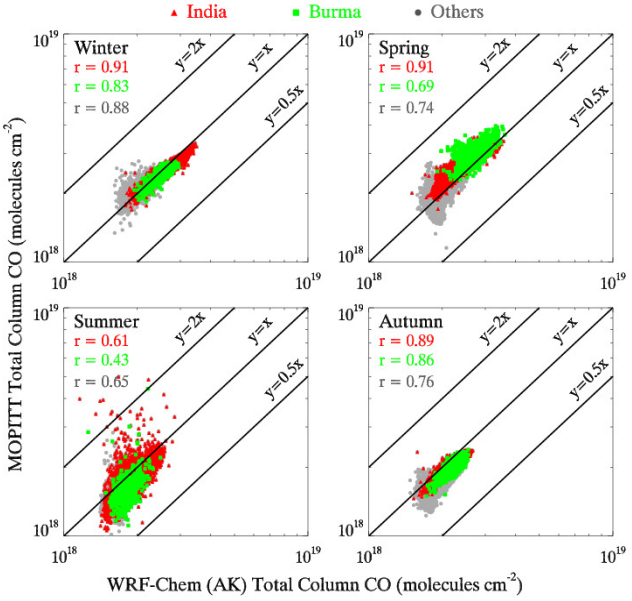

Fig. 10. Scatter plot between seasonally averaged WRF-Chem simulated and MOPITT-retrieved total column CO during winter, spring, summer and autumn of the year 2008. Others correspond to the areas not covered by regions 1–5 shown in Fig. 1. The correlation coefficients for each region are also shown.

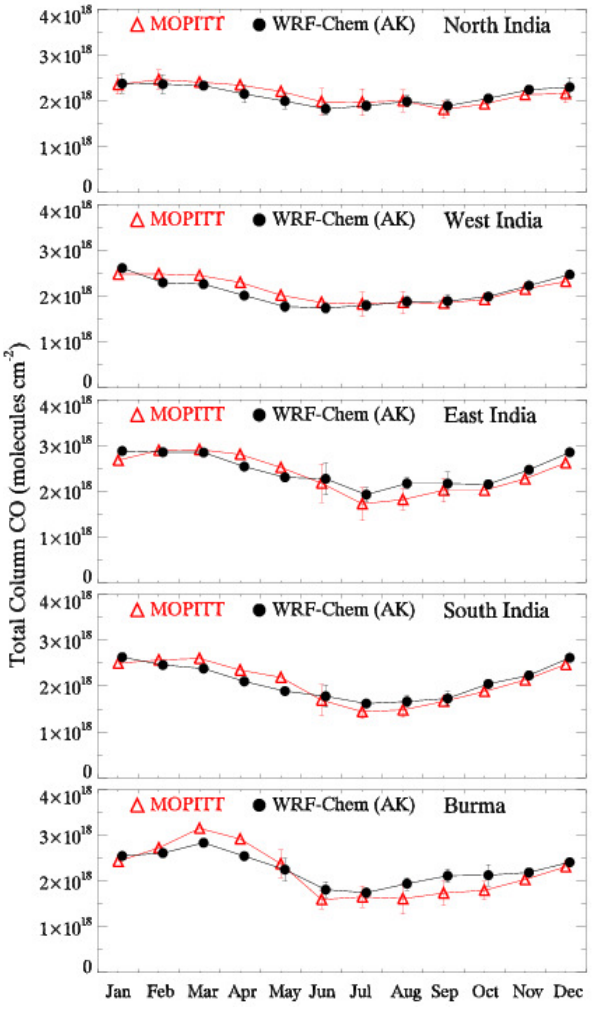

Fig. 11. Seasonal variations in WRF-Chem simulated and MOPITT-retrieved CO total column over the five regions defined in Fig. 1.

4.2.2 Comparison with MOPITT CO retrievals

The spatial distributions of model-simulated and MOPITT-retrieved seasonal mean total column CO during winter, spring, summer and autumn of the year 2008 are shown in Fig. 9. Both model and MOPITT data are averaged over a $0.25° \times 0.25°$ grid. The MOPITT-retrieved total column CO values are mostly representative of the free tropospheric CO, which is the region where MOPITT retrievals have highest sensitivity. The spatial variability as well as the seasonal variation of the MOPITT-retrieved total column CO is reproduced well by the model. In general, both the model and MOPITT are highest during winter, decrease during spring, attain minimum levels during summer and increase again during autumn.

The percentage difference between model and MOPITT relative to MOPITT- retrieved total column CO abundances is also shown in Fig. 9. The model is generally within $\pm 20\,\%$ of MOPITT, but mostly underestimates MOPITT during spring and overestimates MOPITT during other seasons. The monthly variation of different statistical metrics calculated using the co-located WRF-Chem and MOPITT retrievals is shown in Table 3. The index of agreement varies between 0.63 and 0.84, indicating that the model performs generally well in simulating the variations around the MOPITT mean. The model systematically underestimates MOPITT retrievals from February–July with MB ranging from -0.33×10^{17} to -2.21×10^{17} molecules cm^{-2} and overestimates MOPITT during August–January with MB ranging from 0.05×10^{17} to 1.32×10^{17} molecules cm^{-2}. The mean bias is highest during spring (high fire activity season). MNB, RMSE and MNGE also show similar seasonal variability and are estimated to be about 7 to $-9.3\,\%$, 2.38×10^{17} to 3.45×10^{17} molecules cm^{-2} and 8 % to 11 %, respectively.

The relationship between WRF-Chem and MOPITT-retrieved total column CO is further portrayed in terms of scatter plot analysis in Fig. 10. Data over India and Burma are represented by red triangles and green squares, respectively, while data over the other regions are shown as grey filled circles. The correlation coefficients (r) for these regions are estimated to be 0.43 to 0.91 during all the seasons. The agreement between WRF-Chem and MOPITT is better during winter and autumn as compared to spring and summer. Lowest r values during summer could in part be associated with a fewer number of samples due to wide-spread

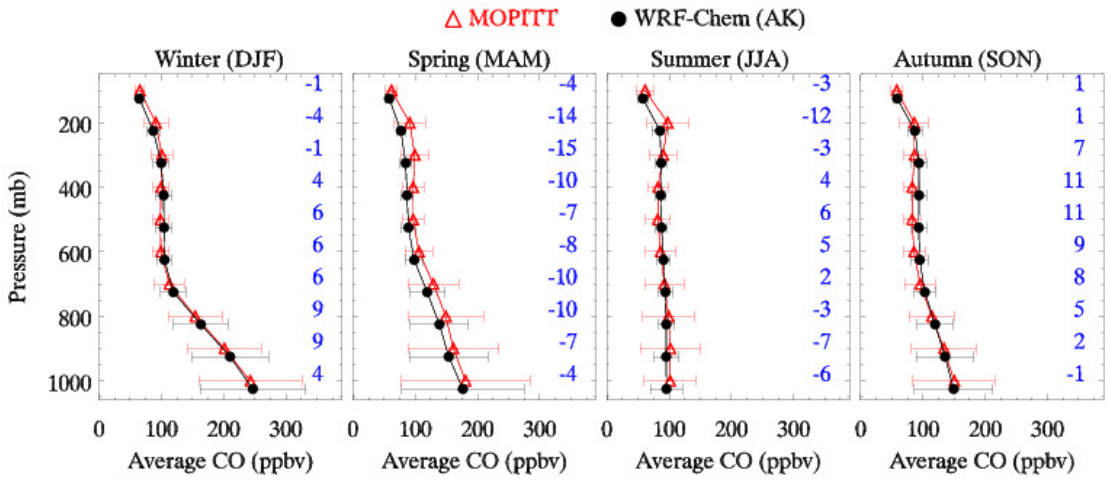

Fig. 12. Comparison of the vertical profiles of CO mixing ratios retrieved by MOPITT and simulated by WRF-Chem during the winter, spring, summer and autumn seasons 2008. WRF-Chem profiles are transformed using MOPITT averaging kernel and a priori profile before this comparison. The vertical profiles are obtained using co-located WRF-Chem and MOPITT data. The difference between WRF-Chem simulated and MOPITT-retrieved average CO value (ppbv) is also shown for each level.

Table 3. Seasonal variation in index of agreement (d), mean bias (MB), mean normalized bias (MNB), root-mean-square error (RMSE) and mean normalized gross error (MNGE) computed using the co-located WRF-Chem and MOPITT-retrieved total CO column values. The total number of data points (N) used in the calculation is also listed.

Month	D	MB[1]	MNB[2]	RMSE[1]	MNGE[2]	N
Jan	0.74	1.18	−5.0	2.58	8.1	146 900
Feb	0.83	−1.13	−4.2	2.71	7.9	116 336
Mar	0.84	−1.77	−6.4	3.45	10.2	179 429
Apr	0.75	−2.21	−8.8	3.66	11.4	189 166
May	0.74	−2.02	−9.3	2.86	10.5	140 377
Jun	0.67	−0.78	−2.8	2.65	9.6	51 872
Jul	0.63	−0.33	−0.1	2.41	9.1	47 443
Aug	0.71	0.05	1.8	2.17	8.9	64 440
Sep	0.69	0.68	5.2	2.22	10.2	117 444
Oct	0.75	1.10	6.9	2.41	10.5	166 349
Nov	0.82	1.08	5.7	2.38	9.0	190 242
Dec	0.78	1.32	6.0	2.71	9.0	152 983

[1] Unit: $\times 10^{17}$ molecules cm^{-2}
[2] Unit: %

cloud cover associated with monsoonal circulation over this region and also due to larger errors in meteorological parameters during summer. WRF-Chem and MOPITT column CO over the entire domain are generally distributed between the $y = 0.5x$ and $y = 2x$ lines. However, MOPITT CO retrievals for both Burma and India are mostly overestimated by WRF-Chem during all the seasons except during spring when they are underestimated. Since biomass burning constitutes the major fraction of total CO emissions over Burma, it is suggested that CO emissions from biomass burning could be slightly underestimated. Additionally, the absence of plume-rise parameterization in the present model simulations can also contribute to underestimation over the biomass burning regions. A sensitivity study showed that inclusion of plume-rise parameterization during April can increase tropospheric column CO by 10–50 % over biomass burning regions. The overestimation of MOPITT CO retrievals during other seasons (characterized by low fire activity) indicates slight overestimation of anthropogenic emissions over this region.

The seasonal variations in the model-simulated and the MOPITT-retrieved total column CO abundances over the defined five regions agree well, as shown in Fig. 11. The seasonal variation in both the model-simulated and MOPITT- retrieved total column CO over Burma are much different from the Indian regions. Total column CO over Burma is highest during March–April, while those over the Indian regions are highest during winter. The March–April maximum in CO over Burma is associated with intense high biomass burning activity during these months. Biomass burning activity over India is also highest during spring, but biomass burning does not increase total column CO values significantly, because CO emissions from biomass burning over the defined four Indian regions are estimated to be lower than the corresponding anthropogenic CO emissions by 2–32 %, while those over Burma are estimated to be higher than the anthropogenic CO emissions by 3–31 %.

In addition to the total CO column, the model-simulated vertical distributions of CO are also compared to MOPITT retrievals for different seasons (Fig. 12). The vertical gradient of MOPITT CO retrievals is captured well by the model during all the seasons with differences on the order of −15 ppb to 12 ppbv. These values are comparable to the bias (<20 ppbv) reported in MOPITT retrievals against in situ aircraft measurements (Emmons et al., 2004).

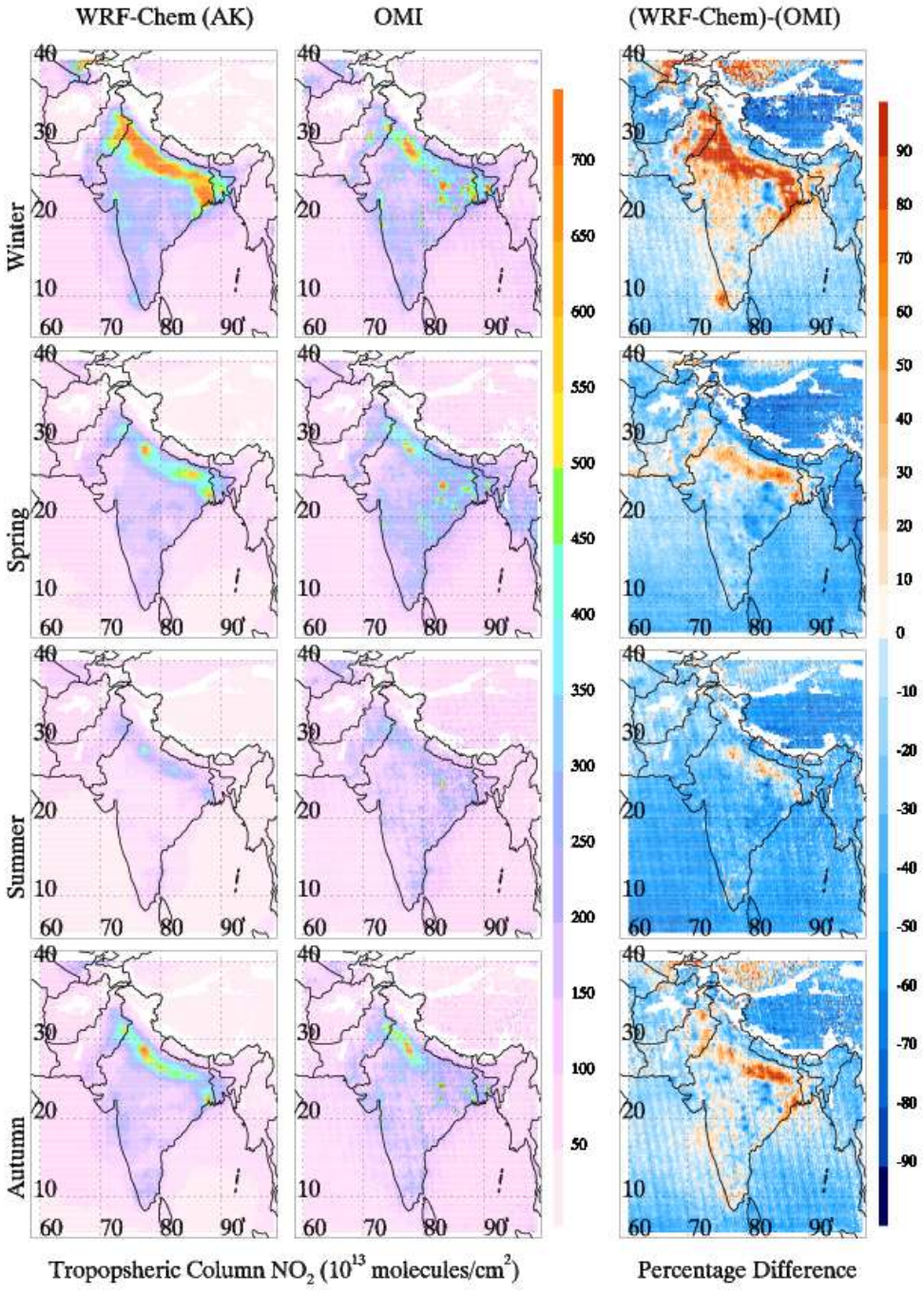

Fig. 13. Spatial distributions of WRF-Chem simulated and OMI- retrieved tropospheric column NO_2 during winter (DJF), spring (MAM), summer (JJA) and autumn (SON) 2008. Note that WRF-Chem profiles are smoothed with OMI averaging kernel before comparison.

4.2.3 Comparison with OMI NO_2 retrievals

The spatial distributions of the model-simulated and OMI-retrieved seasonal mean tropospheric column NO_2 during winter, spring, summer and autumn 2008 are shown in Fig. 13. Both model and OMI data are averaged over a $0.25° \times 0.25°$ grid. Like OMI, the model shows highest tropospheric column NO_2 abundances over the Indo-Gangetic Plain region during all the seasons.

The percentage differences between WRF-Chem and OMI relative to OMI tropospheric column NO_2 (Fig. 13) show that the model tends to overestimate OMI retrievals by 10–50 % over the Indo-Gangetic Plain region with differences as high as 90 % during winter. Percentage difference

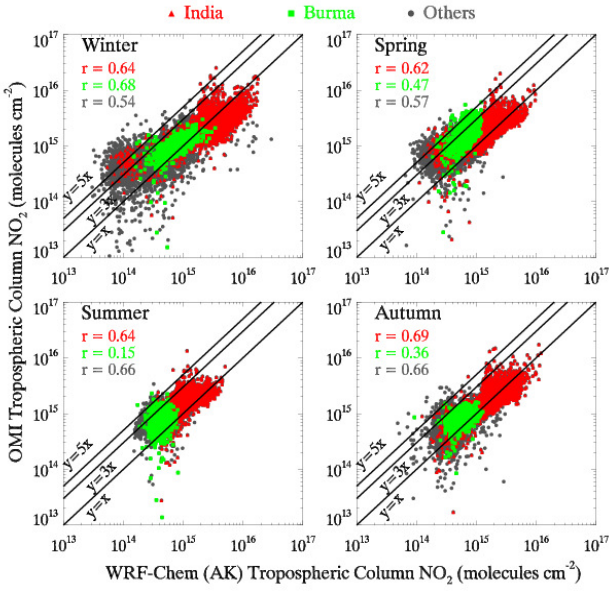

Fig. 14. Scatter plot between seasonally averaged WRF-Chem simulated and OMI-retrieved tropospheric column NO_2 during winter, spring, summer and autumn 2008. Others correspond to the areas not covered by regions 1–5 shown in Fig. 1. The correlation coefficients for each region are also shown.

Table 4. Seasonal variation in index of agreement (d), mean bias (MB), mean normalized bias (MNB), root-mean-square error (RMSE) and mean normalized gross error (MNGE) computed using the co-located WRF-Chem and OMI tropospheric column NO_2 values. The total number of data points (N) used in the calculation is also listed.

Month	d	MB[1]	MNB[2]	RMSE[1]	MNGE[2]	N
Jan	0.61	0.29	271.0	2.36	308.0	271 339
Feb	0.68	0.04	273.6	1.53	313.6	237 513
Mar	0.66	−0.30	201.9	1.41	255.7	278 571
Apr	0.66	−0.33	248.5	1.27	302.6	303 453
May	0.71	−0.49	122.8	1.21	184.7	296 121
Jun	0.64	−0.49	117.0	0.95	189.3	193 869
Jul	0.61	−0.41	141.6	0.77	212.3	194 030
Aug	0.61	−0.36	171.7	0.74	238.3	177 826
Sep	0.66	−0.32	139.7	0.80	200.3	181 364
Oct	0.71	−0.16	268.7	1.04	313.4	250 336
Nov	0.73	−0.03	357.5	1.49	395.5	244 510
Dec	0.72	0.06	314.8	1.83	351.4	235 815

[1] Unit: $\times 10^{15}$ molecules cm^{-2}
[2] Unit: %

values over the rest of the model domain are −50 % to 10 % during all the seasons. The model generally underestimates OMI retrievals during spring and summer, and also over low NOx emission regions during winter and autumn. The monthly statistical analysis of co-located WRF-Chem and OMI tropospheric column NO_2 abundances are listed in Table 4. The index of agreement between model and OMI (0.61–0.73) is smaller than those calculated from the comparison with TES and MOPITT, indicating relatively poor model performance in simulating the NO_2 variability compared to CO and O_3 variability. The estimated MB ranges from -0.03×10^{15} to 0.29×10^{15} molecules = cm^{-2}, and MNB varies between about 117 % and 357 % over the simulation domain. RMSE is estimated as $0.74 \times 10^{15}$to 2.36×10^{15} = molecules = cm^{-2} and MNGE as 184 % to 395 %.

The discrepancies between WRF-Chem and OMI are further illustrated by means of scatter plots in Fig. 14. The scatter plot analysis confirms the systematic underestimation of OMI retrievals by WRF-Chem over most of the domain during all the seasons. Retrieved and modeled tropospheric column NO_2 abundances over India are generally distributed between the y = x and y = 3x lines, i.e. the agreement is within a factor of 3. Over Burma, better agreement is found during winter and autumn (y = 3x), while during spring and summer we find differences up to a factor 5. Such an underestimation by a factor of 2–5 is not surprising and is consistent with results from previous studies over other Asian regions (e.g. Akimoto et al., 2006; Uno et al., 2007), indicating towards higher uncertainties of Asian emissions. The correlation coefficients over these regions are estimated to be 0.36 to 0.69 during all the seasons except over Burma during summer (0.15). The poor agreement between model and OMI during summer over Burma could be related to very low levels ($<1 \times 10^{15}$ mol cm^{-2}) of tropospheric column NO_2 over this region. These low levels are comparable to the retrieval error of $0.5–1.0 \times 10^{15}$ mol cm^{-2} reported for OMI tropospheric column NO_2 (Boersma et al., 2007). Burma is significantly influenced by biomass burning activities during spring (Fig. 3), and larger model-OMI discrepancies in this region are likely due to underestimation of NO_x emissions from fires. Like Burma, the model also underestimates OMI retrievals over other regions influenced by the fires during spring, such as Indian regions due south of 25° N and the Indus Plain in western Pakistan (Figs. 3 and 13). The uncertainties in datasets of fuel load, emission factors, combustion efficiency and burned area are the likely contributors to errors in biomass burning emission inventories, and these errors must be reduced to improve the model performance in regions influenced by intense biomass burning activity. The absence of a plume rise parameterization in the present simulations also contributes to these discrepancies over Burma and other biomass burning regions. A sensitivity analysis conducted by including plume rise parameterization during April showed that this parameterization can increase the tropospheric column NO_2 by more than 100 % over Burma and by 10–50 % over biomass burning regions in India.

The model also underestimates OMI retrievals over the model domain during seasons of low fire activity (summer and autumn), and this indicates that the anthropogenic NO_x

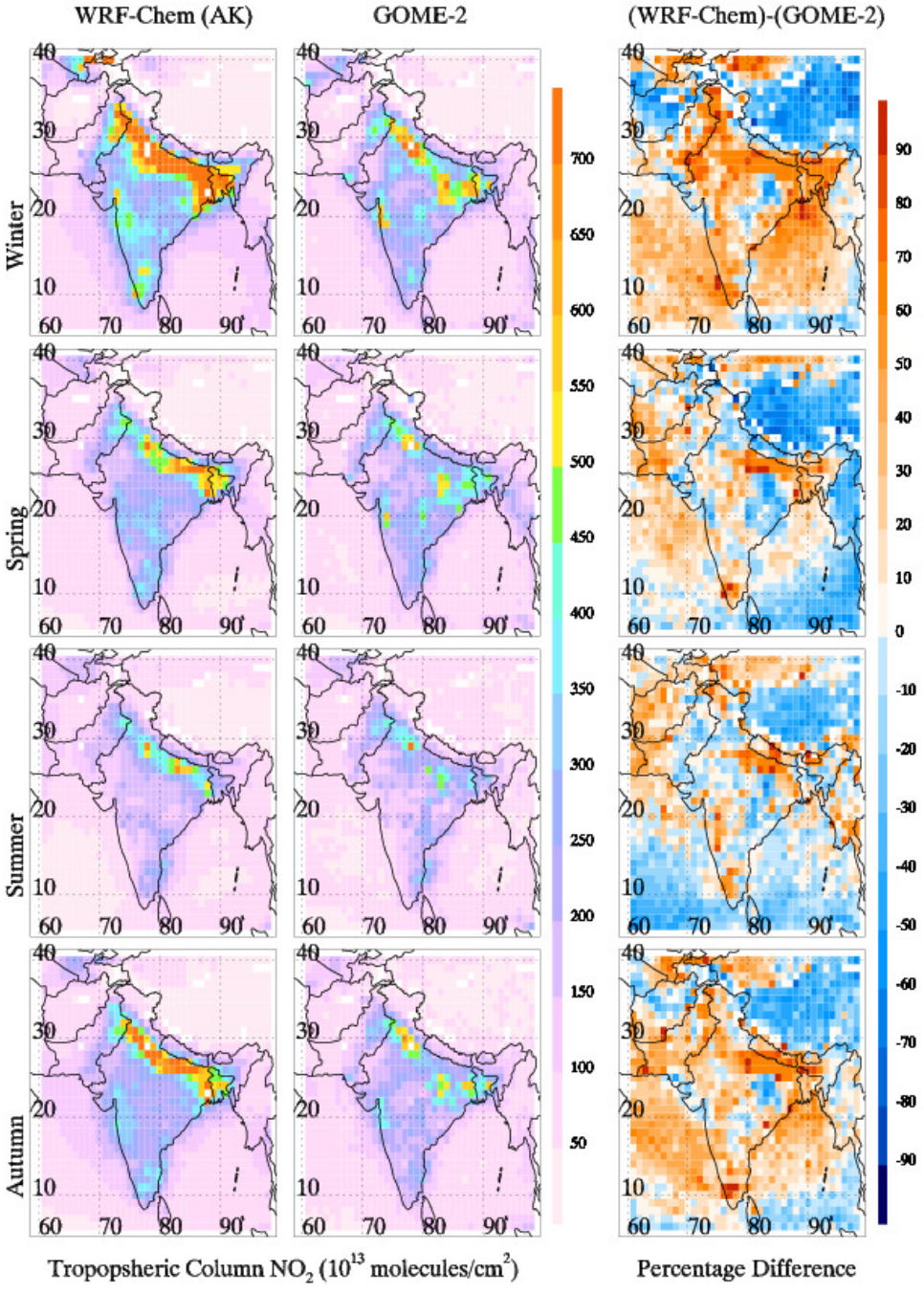

Fig. 15. Spatial distributions of WRF-Chem simulated and GOME-2 retrieved tropospheric column NO_2 during winter (DJF), spring (MAM), summer (JJA) and autumn (SON) 2008. Note that WRF-Chem profiles are smoothed with GOME-2 averaging kernel before comparison.

emissions are underestimated over the South Asian region. The errors in anthropogenic emission estimates arise mainly due to uncertainties in basic energy consumption, emission factors and socio-economic datasets used for constructing emission inventory. In addition to the uncertainties in anthropogenic emission estimates, the use of year 2006 anthropogenic emissions in the present model simulations (year 2008) may also explain some of the discrepancies. Analysis of historical data (1980–2003) from the Regional Emission Inventory for Asia (REAS) shows that Indian NO_x emissions have increased by about 177 % (∼7.7 % per year) from 1980 to 2003 (Ohara et al., 2007). Tropospheric column NO_2 abundances have also shown a positive trend over India from 1996 to 2006 (Ghude et al., 2008).

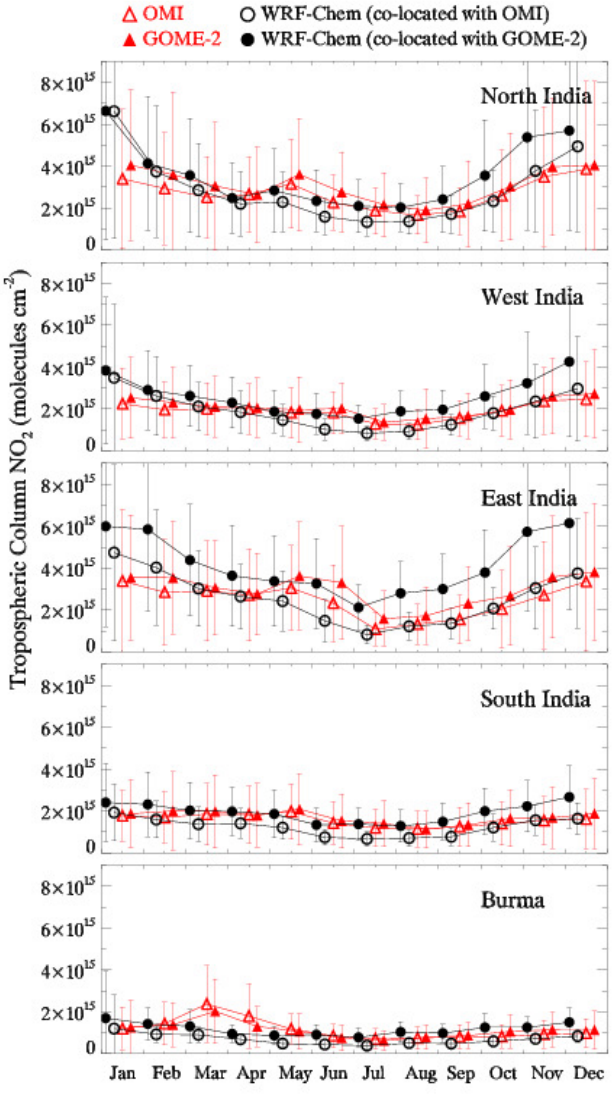

Fig. 16. Seasonal variations in WRF-Chem simulated, OMI and GOME-2 retrieved tropospheric column NO_2 values over the regions defined in Fig. 1.

To examine the impact of the reported increase in anthropogenic emissions from 2006 to 2008, a 10-day sensitivity model run was performed during July with NO_x emissions increased by 15 %. July has low anthropogenic NO_x emissions (Fig. 2a). The sensitivity run shows that increasing the emissions by the reported growth rate increase, the model-simulated tropospheric column NO_2 amounts over inland by 5–15 % during July. Tropospheric column NO_2 over the oceanic regions increases by less than 10 %. The largest increase in tropospheric column NO_2 abundances is seen over the Indo-Gangetic Plain region. While adjusting the emissions for temporal trends does increase the model values, it only accounts for a small part of the differences to OMI retrievals. These results suggest the need for substantial improvements in the anthropogenic NO_x emission inventories in order to accurately simulate the NO_x distribution over South Asia. Some other important sources that can possibly lead to discrepancies are NO_x emissions from microbial activity and lightning, uncertainties in seasonal variations of emissions, and absence of diurnal and vertical profiles of anthropogenic emissions. The MEGAN soil NO_x emissions are estimated to be uncertain, and these uncertainties could add to model-observation discrepancies, especially in rural Indian regions during summer where heavy precipitation events are shown to induce strong pulses of NO_x, amounting to a total of 23–28 ng N m^{-2} s^{-1} (Ghude et al., 2010). Lightning NO_x emissions were not included in the simulations but are suggested to contribute very little to NO_x emissions over the Indian region (Ghude et al., 2010).

To confirm the reality of these large uncertainties in NO_x simulations, the model-simulated tropospheric NO_2 is also compared with GOME-2 retrievals. The spatial distributions of model-simulated and GOME-2 retrieved tropospheric column NO_2 abundances during the four seasons of 2008 are shown in Fig. 15 along with percentage difference between WRF-Chem and GOME-2 relative to GOME-2 retrievals. GOME-2 retrievals and modeled values are averaged over 1°x1° grid because of the larger size (40 km × 80 km) GOME-2 viewing pixel. Like OMI and WRF-Chem, GOME-2 also shows highest tropospheric NO_2 values over the Indo-Gangetic plain during all the seasons. Similar to OMI retrievals, the model also overestimates the GOME-2 retrievals over the Indo-Gangetic Plain region by 10–50 % and generally underestimates them during spring and summer except for a few grid boxes. The model significantly underestimates GOME-2 retrievals over Burma and other biomass burning regions during spring by −10 to −50 % and over the regions of low NO_x emissions. In contrast to OMI retrievals, the model overestimates the GOME-2 retrievals over parts of the Arabian Sea and Bay of Bengal where tropospheric column NO_2 abundances are low ($<1 \times 10^{15}$ molecules cm^{-2}). However, it should be noted that GOME-2 values over these regions are comparable to the error of 0.5–1.0 $\times 10^{15}$ molecules cm^{-2} reported for GOME retrievals.

The seasonal variations in tropospheric NO_2-simulated by WRF-Chem over the defined five regions are compared with co-located OMI and GOME-2 retrievals in Fig. 16. Both OMI and GOME-2 tropospheric NO_2 columns show lower values during summer/monsoon season and increase again during autumn. Model-simulated NO_2 values show a systematic increase during autumn but do not show in springtime higher levels. Highest OMI NO_2 values over India are observed in late autumn–winter while over Burma in March. The seasonal variations in OMI and GOME-2 tropospheric column NO_2 are found to agree well with the seasonal variability of fire counts (not shown) in the respective regions. The largest discrepancies during spring again point to uncertainties in the biomass burning emission estimates apart

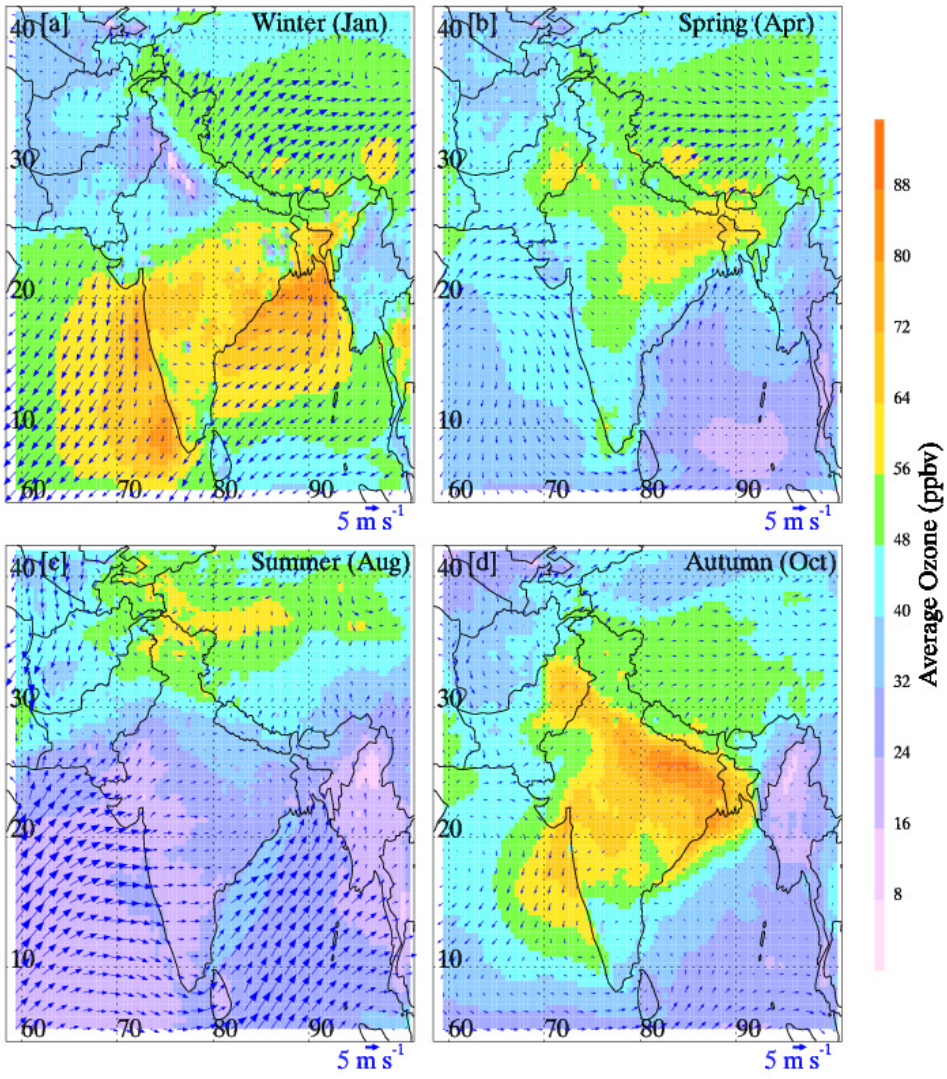

Fig. 17. Spatial distribution of WRF-Chem simulated surface ozone during January, April, August and October of the year 2008. Monthly mean 10 m wind vectors are also shown.

from the uncertainties in anthropogenic emission estimates. Interestingly, WRF-Chem values are closer to OMI retrievals than GOME-2, but similar variations in both the WRF-Chem datasets (co-located with OMI and GOME-2) indicate that differences estimated between model and satellite retrievals and the inferences drawn about the NO_x emissions from these differences may be real.

The evaluation results confirm that the model is capable of reproducing many of the observed patterns and overall captures the seasonal variation in surface ozone and CO across the Indian region. The evaluation against TES and MOPITT satellite retrievals also lends confidence to the model's ability in simulating general seasonal patterns of lower tropospheric ozone and total column CO. Regional differences in the seasonal variations of ozone, CO and NO_2 are also reproduced by the model. While there are weaknesses in the model performance, e.g. in representing the magnitude and seasonality of NO_2 columns, the evaluation results give confidence that the model provides meaningful information to examine the spatio-temporal distribution of surface ozone over India.

4.3 Analysis of modeled surface ozone

The spatial distributions of model-simulated monthly mean surface ozone during January, April, August and October (representing winter, spring, summer and autumn) over South Asia, along with 10 m wind vectors, are depicted in Fig. 17. During January, ozone levels are highest (>55 ppbv) over central and eastern parts of India, the Arabian Sea along the coast and the northern Bay of Bengal. Interestingly, ozone values along the coasts during January are higher than those over land. This indicates en-route additional

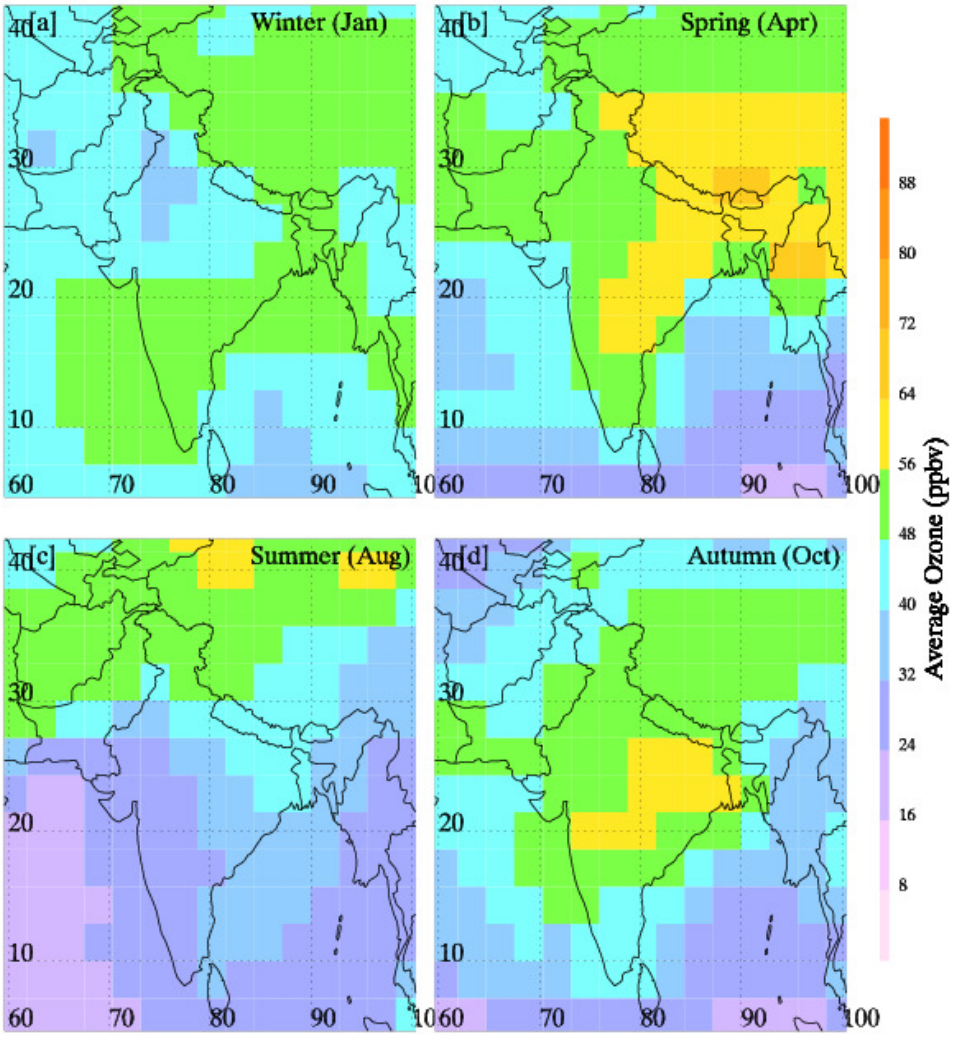

Fig. 18. Spatial distribution of MOZART-simulated surface ozone during January, April, August and October of the year 2008.

photochemical ozone production in offshore continental polluted air due to strong tropical solar radiation and effects of marine boundary layer. The marine boundary layer suppresses the loss of pollutants associated with ventilation and dry deposition due to its shallower and less turbulent nature. In addition, subsidence of ozone-rich free tropospheric air during nighttime could also increase ozone levels in the marine boundary layer. Higher ozone levels simulated over these oceanic regions are consistent with the observations made during INDOEX (e.g. Naja et al., 1999; Lal and Lawrence, 2001; Stehr et al., 2002) and other ship cruises (e.g. Naja et al., 2004; Srivastava et al., 2011). A small region of ozone values less than 16 ppbv is also discerned over northern India during January, which is likely due to lower solar radiation and titration of ozone by higher NO_x levels, as indicated by analysis of modeled solar radiation and NO_x values and also higher anthropogenic NO_x emissions in this region (Fig. 1). Ozone values over the Tibetan Plateau are also higher (45–65 ppbv) than those over the adjacent northern Indian IGP areas.

Moving to spring, modeled ozone remains high in eastern India and increases in northern parts of India, but the high ozone concentrations in southern India and along the coast disappear. This is associated with changes in wind patterns from offshore to onshore, which transports cleaner marine air masses to the inland regions. It should be mentioned that ozone values during spring may be underestimated due to underestimation of CO and NO_x concentrations by the model (Sect. 4.2). Lowest ozone values are simulated for August with average surface ozone not exceeding 40 ppbv over most of India. The levels of ozone precursors are also found to be low during August (Figs. 11 and 16). The strong inflow of marine air masses into the Indian region leads to the development of cloudy and rainy conditions, which, in turn,

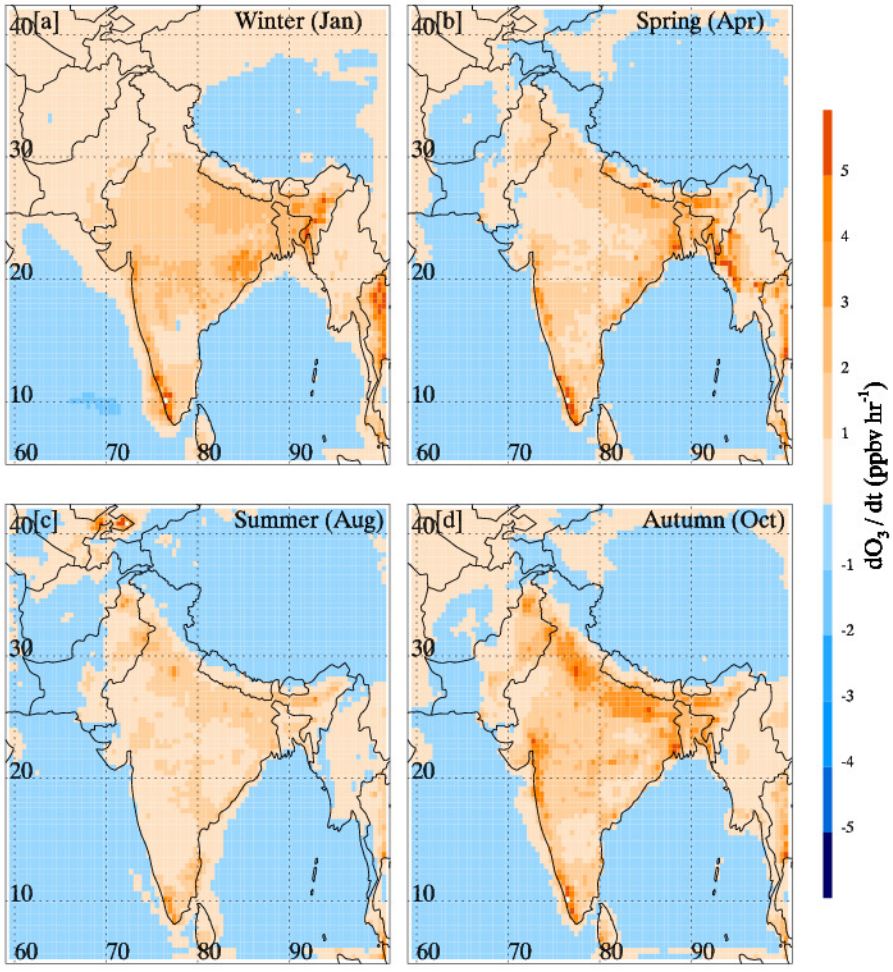

Fig. 19. Spatial distributions of WRF-Chem simulated daytime (11:30–15:30 LT) ozone net production during January, April, August and October 2008.

reduces the solar radiation and suppresses photochemical ozone production during August. Lower levels of ozone precursors may be associated with washout (HNO_3) and vertical transport (CO) to higher altitudes induced by deep convection (e.g. Fu et al., 2006; Park et al., 2007). The marine air masses do not influence the regions north of 30° N, and thus higher ozone values (>55 ppbv) are still seen in those regions and over Tibetan Plateau.

During October, modeled ozone again increases over nearly the entire Indian region and over the entire Indo-Gangetic Plain (IGP) and central India, reaching the seasonal peak. Highest ozone mixing ratios (70–80 ppbv) are seen over the eastern part of the IGP. This increase is associated with an increase in solar radiation and ozone precursors concentrations associated with a change in wind patterns from onshore to offshore. Like January, the offshore transport of pollutants leads to higher ozone mixing ratios along the coastal regions. The spatial distributions of MOZART-simulated surface ozone during January, April, August and October over the model domain are shown in Fig. 18. The spatial and temporal variability of MOZART ozone is nearly similar to the WRF-Chem ozone during all the months. MOZART shows a slight increase from winter–spring over eastern side, particularly in China. WRF-Chem simulates larger range (8–80 ppbv) of ozone values over the Indian region as compared to MOZART (24–72 ppbv), indicating that WRF-Chem is better at capturing small-scale processes due to its higher resolution. The reduction in ozone levels during summer is also captured relatively well by WRF-Chem compared to MOZART, as also evident from Fig. 4. However, more observations with good spatial and temporal coverage are required to evaluate the performance of these models as well as their performance against each other.

To gain further insights into the spatial and temporal variability of surface ozone, the ozone net production (ONP) due to photochemistry is estimated for daytime (11:30–15:30 LT) over the model domain. ONP is calculated as the difference

between gross ozone formation (P (O_3)) and loss (L (O_3)) rates, given by the following equations:

$$P[O_3] = k_1[HO_2][NO] + \sum_i k_{2i}[RO_2]_i[NO]_i \quad (4)$$

$$l[O_3] = k_3[O(^1D)][H_2O] + k_4[OH][O_3] + k_5[HO_2](O_3) \quad (5)$$

where $k_1 - k_5$ represent the rate coefficients of the $HO_2 + NO$, $RO_2 + NO$, $O(^1D) + H_2O$, $OH + O_3$ and $HO_2 + O_3$ reactions, and ϕ is the yield of NO_2 from $RO_2 + NO$ reaction. The spatial distributions of average daytime ONP during January, April, August and October over the model domain are depicted in Fig. 19. In general, ONP values are positive over land and negative over the oceanic and parts of the Himalayan regions during all seasons. Positive ONP values arise due to dominance of ozone production from the combination of higher levels of ozone precursors and strong daytime solar radiation. Positive ONP values are also discerned along the coast in January and October, indicating net daytime ozone production in the continental outflow even over oceanic regions. ONP values remain between 0 and -1 ppbv h^{-1} during daytime over the cleaner environments.

During January, ONP values are highest over central-eastern and coastal regions of India with magnitudes of 2–5 ppbv h^{-1} and are within 0–2 ppbv h^{-1} over other parts of India and Burma. Positive ONP values with magnitudes less than 2 ppbv h^{-1} are also observed over the regions of the Arabian Sea and the Bay of Bengal, experiencing outflow of continental air. Positive ONP values over these oceanic regions disappear during April due to the reversal in wind patterns. ONP values show an increase of about 1 ppbv h^{-1} over northern parts of IGP and slight decrease over central India during April. Lowest ONP values are estimated in August with magnitudes less than about 2 ppbv h^{-1} over most of India. The low ONP values again indicate suppression of photochemical activity during August (monsoon season). In October, ONP values increase by a factor of 2–3 over the entire Indian region relative to August due to increased solar radiation and reversed wind patterns. Daytime ONP values during October reach up to 4–5 ppbv h^{-1} over the IGP region. Net daytime ozone production in the outflow regions over the Arabian Sea is also seen during October. These results clearly indicate that the spatial and seasonal patterns of surface ozone over South Asia are determined by photochemical net ozone production and closely linked to the varying influence of marine air masses associated with monsoonal circulation.

The model results are further used to examine the relative importance of NO_x and NMHCs in ozone production over South Asia. Sillman (1995) showed that model-simulated afternoon ratios of CH_2O to NO_y, H_2O_2 to HNO_3 and O_3 to (NO_y–NO_x) are very useful indicators of the ozone production regime. The critical values of the ratios CH_2O/NO_y, H_2O_2/HNO_3 and $O_3/(NO_y–NO_x)$ separating the two ozone production regimes, are suggested to be 0.28, 0.4 and 7, respectively with lower values indicating a VOC-limited regime, while higher values correspond to a NO_x-sensitive regime (Sillman, 1995). CH_2O/NO_y has been successfully used to distinguish ozone production regimes over the urban areas of Shanghai (Geng et al., 2007) and Mexico (Tie et al., 2007).

The spatial distributions of the simulated monthly average afternoon (11:30–14:30 LT) CH_2O to NO_y ratio during January, April, August and October 2008 are shown in Fig. 20. The ratio is less than 0.28 over some parts of the IGP during winter, indicating hydrocarbon-limited ozone production regime over this region. The rest of the Indian region appears to be NO_x-limited throughout the year. Interestingly, the ratio is seen to be lower over the shipping routes in the Arabian Sea and Indian Ocean, reflecting the critical role of shipping NO_x emissions in ozone production over the cleaner marine regions. The H_2O_2/HNO_3 ratio (not shown) is estimated to be less than 0.4 only in a few grid cells over the IGP region during October, and the $O_3/(NO_y–NO_x)$ (not shown) is estimated to be greater than 7 over the region for all seasons. These results confirm the dominance of a NO_x-limited ozone production regime over India. NO_x-limited ozone production over South Asia might be associated with the fact that emissions in this region are influenced largely by incomplete combustion processes, particularly by biofuel burning, and thus have higher NMHC to NO_x emission ratio as compared to other regions of the Northern Hemisphere (Lawrence and Lelieveld, 2010). Earlier, it was also shown using observed ozone-CO and ozone-NO_x correlation over some of the sites that the emissions of ozone precursors and thus ozone levels are largely determined by incomplete combustion processes (Naja and Lal, 2002; Naja et al., 2003). The sensitivity runs performed by increasing NO_x emissions over the model domain by 15 % and 30 % did not alter the ozone production regime substantially, except for some regions in northern India where ozone production regime changed from NO_x-limited to NMHC-limited. The decrease in CH_2O to NO_y ratios is, however, observed over the whole domain with the increase in NO_x emissions.

5 Discussions and summary

The Weather Research and Forecasting model with Chemistry (WRF-Chem) has been used, for the first time, to simulate the spatial and temporal variability of tropospheric ozone and related species over the South Asian region for the year 2008. Anthropogenic emissions of different species are provided to the model by inserting a regional emission inventory (INTEX-B) into a global emission inventory (RETRO). Daily varying emissions from biomass burning are calculated using MODIS-derived fire locations, while biogenic emissions are calculated online within the model using MEGAN. Model- simulated ozone, carbon monoxide and

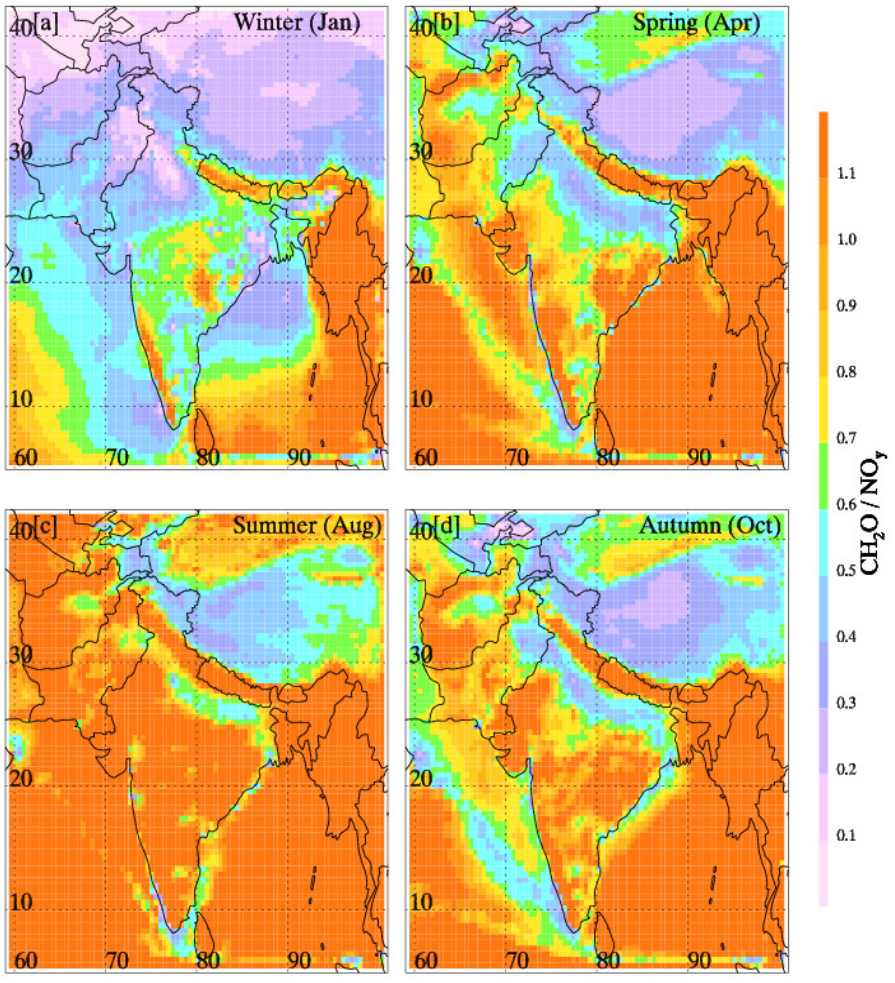

Fig. 20. Spatial distributions of WRF-Chem simulated afternoon (11:30–14:30 LT) CH_2O to NO_y ratio during January, April, August and October of the year 2008.

nitrogen oxides are compared with co-located ground-based, balloon-borne and space-borne observations. Ground-based observations include surface ozone from seven sites and CO and NO_x observations from three sites, while balloon-borne observations are available from two sites in the Indian region. Space-borne observations include retrievals of ozone from TES, nitrogen dioxide from OMI and GOME, and carbon monoxide from MOPITT. The errors and biases in model simulation are quantified through a set of statistical metrics.

The evaluation results indicate that the model has a good ability of simulating the seasonal variations of surface ozone and CO over the Indian region but shows some differences for NO_x seasonality, particularly during spring. The vertical distribution of ozone is also simulated well by the model. The index of agreement, between model simulations and satellite retrievals from TES, OMI and MOPITT, is estimated to be 0.47–0.9, indicating that WRF-Chem is capable of reproducing the overall spatial and temporal variability of ozone, CO and NO_2. However, bias analysis indicates that TES-retrieved lower tropospheric ozone values and OMI- retrieved tropospheric column NO_2values are underpredicted by the model during all seasons. MOPITT total column CO retrievals are underpredicted during February–July, while they are overestimated during other months. The largest differences between model and observations are seen during spring, which is also the season of intense biomass burning activity and is related to uncertainties in the emissions and the treatment of biomass burning sources. Large discrepancies between model and OMI tropospheric column NO_2 abundances for seasons other than spring also point towards large uncertainties in anthropogenic NO_x emission estimates. A sensitivity simulation employing a plume rise parameterization for biomass burning emissions showed significant enhancement in tropospheric CO and NO_x over biomass burning regions.

Chemical and meteorological model fields are used to understand the spatio-temporal variability of surface ozone, and the analysis clearly indicates regional differences in the

seasonality of surface ozone over South Asia. The inland regions show net ozone production (0 to 5 ppbv h^{-1}), while the cleaner marine and mountainous regions show net ozone destruction (0 to -2 ppbv h^{-1}) during daytime. Net ozone production (0–2 ppbv h^{-1}) is also seen over the marine regions experiencing outflow from the South Asian region. Highest net ozone production rates are seen over the Indo-Gangetic Plain (IGP) region and in some cities located along the coastal regions of India. Ozone production over South Asia is estimated to be limited mostly by NO_x except for some regions over the Indo-Gangetic Plain region during winter.

This study lends confidence to the use of WRF-Chem for analyzing the spatial and temporal variability in trace gases over India. Differences in modeled- and satellite-retrieved values of ozone and its precursors are due to a number of factors (e.g. model transport and chemistry, coarse model resolution, errors in satellite retrievals, etc.), but uncertainties in CO and NO_x emission estimates over this region are the largest uncertainty. It is essential to improve the emission estimates over this region, as these uncertainties will lead to errors in simulating the ozone production over South Asia, which in turn will pose a major limitation to regional air quality management. It is also highly desirable to have extensive ground-based observations in South Asia, particularly in northern India where air quality is poor and the conditions are more complex due to highly complex terrain of the Indo-Gangetic Plain and Himalayan region. Much more validation of space-borne observations using ground-based instruments also needs to be conducted for the India region. Detailed and focused modeling work together with an increased number of observations will enable a better understanding of tropospheric chemistry and current and future air quality over India, which is presently lacking.

Supplementary material related to this article is available online at: http://www.geosci-model-dev.net/5/619/2012/gmd-5-619-2012-supplement.pdf.

Acknowledgements. M. Naja and R. Kumar are thankful to Shyam Lal, Ram Sagar and C. B. S. Dutt for their keen interest in this work and acknowledge support from ISRO-ATCTM project. R. Kumar is also thankful to Sachin Ghude for fruitful discussions. We are also thankful to Louisa Emmons and Helen Worden for their help and fruitful discussions. The datasets for boundary conditions, biogenic emissions and the programs used to process these datasets are downloaded from the website http://www2.acd.ucar.edu/wrf-chem/. We also thank the teams of MOPITT, OMI and TES for making available data of CO, NO_2 and ozone, respectively. The National Center for Atmospheric Research is supported by the National Science Foundation. We thank three anonymous reviewers for their constructive comments and suggestions.

Edited by: T. Butler

References

Ackermann, I. J., Hass, H., Memmesheimer, M., Ebel, A., Binkowski, F. S., and Shankar, U.: Modal aerosol dynamics model for Europe: development and first applications, Atmos. Environ., 32, 2981–2999, 1998.

Akimoto, H.: Global air quality and pollution, Science, 302, 1716–1719, doi:10.1126/science.1092666, 2003.

Akimoto, H., Ohara, T., Kurokawa, J., and Horri, N.: Verification of energy consumption in China during 1996–2003 by using satellite observational data, Atmos. Environ., 40, 7663–7667, doi:10.1016/j.atmosenv.2006.07.052, 2006.

Allen, D., Pickering, K., and Fox-Rabinovitz, M.: Evaluation of pollutant outflow and CO sources during TRACE-P using model-calculated, aircraft-based and Measurements of Pollution in the Troposphere (MOPITT)-derived CO concentrations, J. Geophys. Res., 109, D15S03, doi:10.1029/2003JD004250, 2004.

Beer, R., Glavich, T. A., and Rider, D. M.: Tropospheric Emission Spectrometer for the Earth Observing System's Aura satellite, Appl. Opt., 40, 2356–2367, 2001.

Beig, G., Gunthe, S., and Jadhav, D. B.: Simultaneous measurements of ozone and its precursors on a diurnal scale at a semi urban site in India, J. Atmos. Chem., doi:10.1007/s10874-007-9068-8, 2007.

Beig, G. and Brasseur, G. P.: Influence of anthropogenic emissions on tropospheric ozone and its precursors over the Indian tropical region during a monsoon, Geophys. Res. Lett., 33, L07808, doi:10.1029/2005GL024949, 2006.

Boersma, K. F., Eskes, H. J., Veefkind, J. P., Brinksma, E. J., van der A, R. J., Sneep, M., van den Oord, G. H. J., Levelt, P. F., Stammes, P., Gleason, J. F., and Bucsela, E. J.: Near-real time retrieval of tropospheric NO_2 from OMI, Atmos. Chem. Phys., 7, 2103–2118, doi:10.5194/acp-7-2103-2007, 2007.

Boersma, K. F., Jacob, D. J., Bucsela, E. J., Perring, A. E., Dirksen, R., vander A, R. J., Yantosca, R. M., Park, R. J., Wenig, M. O., Bertram, T. H., and Cohen, R. C.: Validation of OMI tropospheric NO_2 observations during INTEX-B and application to constrain NO_x emissions over the eastern United States and Mexico, Atmos. Environ., 42, 4480–4497, 2008.

Boersma, K. F., Jacob, D. J., Trainic, M., Rudich, Y., DeSmedt, I., Dirksen, R., and Eskes, H. J.: Validation of urban NO_2 concentrations and their diurnal and seasonal variations observed from the SCIAMACHY and OMI sensors using in situ surface measurements in Israeli cities, Atmos. Chem. Phys., 9, 3867–3879, doi:10.5194/acp-9-3867-2009, 2009a.

Boersma, K. F., Dirksen, R. J., Veefkind, J. P., Eskes, H. J., and van der A, R. J.: Dutch OMI NO_2 (DOMINO) data product, HE5 data file user manual, http://www.temis.nl/docs/OMI_NO2_HE5_1.0.2.pdf, 2009b.

Bowman, K. W., Steck, T., Worden, H. M., Worden, J., Clough, S., and Rodgers, C.: Capturing time and vertical variability of tropospheric ozone: A study using TES nadir retrievals, J. Geophys. Res., 107, 4723, doi:10.1029/2002JD002150, 2002.

Bucsela, E. J., Celarier, E. A., Wenig, M. O., Gleason, J. F., Veefkind, J. P., Boersma, K. F., and Brinksma, E. J.: Algorithm for NO_2 vertical column retrieval from the ozone monitoring instrument, IEEE T. Geosci. Remote, 44, 1245–1258, 2006.

Celarier, E. A. and Retscher, C.: OMNO2e Data product Readme File, Document Revision 1.2, NASA Goddard Space Flight Center, http://toms.gsfc.nasa.gov/omi/no2/OMNO2e_DP_Readme.pdf, 2009.

Cooper, O. R., Parrish, D. D., Stohl, A., Trainer, M., Nédélec, P, Thouret, V., Cammas, J. P., Oltmans, S. J., Johnson, B. J., Tarasick, D., Leblanc, T., McDermid, I. S., Jaffe, D., Gao, R., Stith, J., Ryerson, T., Aikin, K., Campos, T., Weinheimer, A., and Avery, M. A.: Increasing springtime ozone mixing ratios in the free troposphere over western North America, Nature, 463, 344–348, 2010.

David, L. M. and Nair, P. R.: Diurnal and seasonal variability of surface ozone and NO_X at a tropical coastal site: Association with mesoscale and synoptic meteorological conditions, J. Geophys. Res., 116, D10303, doi: 10.1029/2010JD015076, 2011.

Decesari, S., Facchini, M. C., Carbone, C., Giulianelli, L., Rinaldi, M., Finessi, E., Fuzzi, S., Marinoni, A., Cristofanelli, P., Duchi, R., Bonasoni, P., Vuillermoz, E., Cozic, J., Jaffrezo, J. L., and Laj, P.: Chemical composition of PM10 and PM1 at the high-altitude Himalayan station Nepal Climate Observatory-Pyramid (NCO-P) (5079 m a.s.l.), Atmos. Chem. Phys., 10, 4583–4596, doi:10.5194/acp-10-4583-2010, 2010.

Deeter, M. N., Emmons, L. K., Francis, G. L., Edwards, D. P., Gille, J. C., Warner, J. X., Khattatov, B., Ziskin, D., Lamarque, J.-F., Ho, S.-P., Yudin, V., Attié, J.-L., Packman, D., Chen, J., Mao, D., and Drummond, J. R.: Operational carbon monoxide retrieval algorithm and selected results for the MOPITT instrument, J. Geophys. Res., 108, 4399, doi:10.1029/2002JD003186, 2003a.

Deeter, M. N.: MOPITT (Measurements of Pollution in the Troposphere), Validated Version 4 Product User's Guide, MOPITT Algorithm Development Team, Atmospheric Chemistry Division, National Center for Atmospheric Research, Boulder, 18–19, 2003b.

Deeter, M. N., Emmons, L. K., Edwards, D. P., Gille, J. C., and Drummond, J. R.: Vertical resolution and information content of CO profiles retrieved by MOPITT, Geophys. Res. Lett., 31, L15112, doi:10.1029/2004GL020235, 2004.

Emmons, L. K., Deeter, M. N.,Gille, J. C., Edwards, D. P., Attié, J.-L., Warner, J., Ziskin, D., Francis, G., Khattatov, B., Yudin, V., Lamarque, J.-F., Ho, S.-P., Mao, D., Chen, J. S., Drummond, J., Novelli, P., Sachse, G., Coffey, M. T., Hannigan, J. W., Gerbig, C., Kawakami, S., Kondo, Y., Takegawa, N., Schlager, H., Baehr, J., and Ziereis, H.: Validation of Measurements of Pollution in the Troposphere (MOPITT) CO retrievals with aircraft in situ profiles, J. Geophys. Res., 109, D03309, doi:10.1029/2003JD004101, 2004.

Emmons, L. K., Pfister, G. G., Edwards, D. P., Gille, J. C., Sachse, G., Blake, D., Wofsy, S., Gerbig, C., Matross, D., and Nédélec, P.: Measurements of Pollution in the Troposphere (MOPITT) validation exercises during summer 2004 field campaigns over North America, J. Geophys. Res., 112, D12S02, doi:10.1029/2006JD007833, 2007.

Emmons, L. K., Edwards, D. P., Deeter, M. N., Gille, J. C., Campos, T., Nédélec, P., Novelli, P., and Sachse, G.: Measurements of Pollution In The Troposphere (MOPITT) validation through 2006, Atmos. Chem. Phys., 9, 1795–1803, doi:10.5194/acp-9-1795-2009, 2009.

Emmons, L. K., Walters, S., Hess, P. G., Lamarque, J.-F., Pfister, G. G., Fillmore, D., Granier, C., Guenther, A., Kinnison, D., Laepple, T., Orlando, J., Tie, X., Tyndall, G., Wiedinmyer, C., Baughcum, S. L., and Kloster, S.: Description and evaluation of the Model for Ozone and Related chemical Tracers, version 4 (MOZART-4), Geosci. Model Dev., 3, 43–67, doi:10.5194/gmd-3-43-2010, 2010.

Engardt, M.: Modelling of near-surface ozone over South Asia, J. Atmos. Chem., 59, 61–80, doi:10.1007/s10874-008-9096-z, 2008.

Fu, R., Hu, Y., Wright, j. S., Jiang, J. H., Dickinson, R. E., Chen, M., Filipiak, M., Read, W. G., Waters, J. W., Wu, D. L.: Short circuit of water vapor and polluted air to the global stratosphere by convective transport over the Tibetan Plateau, Proc. Natl. Acad. Sci. USA, 103, 5664–5669, 2006.

Geng, F., Zhao, C., Tang, X., Lu, G., and Tie, X.: Analysis of ozone and VOCs measured in Shanghai: A case study, Atmos. Environ., 41, 989–1001, 2007.

Ghude, S. D., Fadnavis, S., Beig, G., Polade, S. D., and van der A, R. J.: Detection of surface emissions hot spots, trends, and seasonal cycle from satellite-retrieved NO_2 over India, J. Geophys. Res., 113, D20305, doi: 10.1029/2007JD009615, 2008.

Ghude, S. D., Lal, D. M., Beig, G., van der A, R., and Sable, D.: Rain-Induced Soil NO_X Emissions from India During the Onset of the Summer Monsoon: A SatellitePerspective, J. Geophys. Res., 115, D16304, doi: 10.1029/2009JD013367, 2010.

Grell, G. A., Peckham, S. E., Schmitz, R., McKeen, S. A., Frost, G., Skamarock, W. C., and Eder, B.: Fully coupled "online" chemistry within the WRF model, Atmos. Environ., 39, 6957–6975, 2005.

Guenther, A., Karl, T., Harley, P., Wiedinmyer, C., Palmer, P. I., and Geron, C.: Estimates of global terrestrial isoprene emissions using MEGAN (Model of Emissions of Gases and Aerosols from Nature), Atmos. Chem. Phys., 6, 3181–3210, doi:10.5194/acp-6-3181-2006, 2006.

Han, K. M., Song, C. H., Ahn, H. J., Park, R. S., Woo, J. H., Lee, C. K., Richter, A., Burrows, J. P., Kim, J. Y., and Hong, J. H.: Investigation of NOx emissions and NO_X-related chemistry in East Asia using CMAQ-predicted and GOME-derived NO2 columns, Atmos. Chem. Phys., 9, 1017–1036, doi:10.5194/acp-9-1017-2009, 2009.

Harris, N., Hudson, R., and Phillips, C.: Assessment of Trends in the Vertical Distribution of ozone, SPARC Report No. 1, WMO Ozone Research and Monitoring Project Report No. 43, 1998.

He, Y. J., Uno, I., Wang, Z. F., Pochanart, P., Li, J., and Akimoto, H.: Significant impact of the East Asia monsoon on ozone seasonal behavior in the boundary layer of Eastern China and the west Pacific region, Atmos. Chem. Phys., 8, 7543–7555, doi:10.5194/acp-8-7543-2008, 2008.

Hegde, P., Pant, P., Naja, M., Dumka, U. C., and Sagar, R.: South Asian dust episode in June 2006: Aerosol observations in the central Himalayas, Geophys. Res. Lett., 34, L23802, doi:10.1029/2007GL030692, 2007.

Herron-Thorpe, F. L., Lamb, B. K., Mount, G. H., and Vaughan, J. K.: Evaluation of a regional air quality forecast model for tropospheric NO_2 columns using the OMI/Aura satellite tropospheric NO2 product, Atmos. Chem. Phys., 10, 8839–8854,

doi:10.5194/acp-10-8839-2010, 2010.

Jain, S. L., Arya, B. C., Kumar, A., Ghude, S. D., and Kulkarni, P. S.: Observational study of surface ozone at New Delhi, India, Int. J. Remote Sens., 26, 3515–3524, 2005.

Kleinman, L., Lee, Y.-N., Springston, S. R., Nunnermacker, L., Zhou, A., Brown, R., Hallock, K., Klotz, P., Leahy, D., Lee, J. H., Newman, L.: Ozone formation at a rural site in the southern United States, J. Geophys. Res., 99, 3469–3482, 1994.

Kramer, L. J., Leigh, R., Remedios, J. J., and Monks, P. S.: Comparison of OMI and ground-based in situ and MAX-DOAS measurements of tropospheric nitrogen dioxide in an urban area, J. Geophys. Res., 113, D16S39, doi: 10.1029/2007JD009168, 2008.

Kumar, R., Naja, M., Venkataramani, S., and Wild, O.: Variations in surface ozone at Nainital, a high altitude site in the Central Himalayas, J. Geophys. Res., 115, D16302, doi:10.1029/2009JD013715, 2010.

Kumar, R., Naja, M., Pfister, G. G., Barth, M. C., and Brasseur, G. P.: Simulations over South Asia using the Weather Research and Forecasting model with Chemistry (WRF-Chem): set-up and meteorological evaluation, Geosci. Model Dev., 5, 321–343, doi:10.5194/gmd-5-321-2012, 2012.

Kunhikrishnan, T., Lawrence, M. G., von Kuhlmann, R., Wenig, M. O., Asman, W. A. H., Richter, A., and Burrows J. P.: Regional NO_x emission strength for the Indian subcontinent and the impact of emissions from India and neighboring countries on regional O_3 chemistry, J. Geophys. Res., 111, D15301, doi:10.1029/2005JD006036, 2006.

Lal, S., Naja, M., and Jayaraman, A.: Ozone in the marine boundary layer over the tropical Indian Ocean, J. Geophys. Res., 103, 18907–18917, 1998.

Lal, S. and Lawrence, M. G.: Elevated mixing ratios of surface ozone over the Arabian Sea, Geophys. Res. Lett., 28, 1487–1490, 2001.

Lal, S., Naja, M., and Subbaraya, B. H.: Seasonal variations in surface ozone and its precursors over an urban site in India, Atmos. Environ., 34, 2713–2724, 2000.

Lawrence, M. G. and Lelieveld, J.: Atmospheric pollutant outflow from southern Asia: a review, Atmos. Chem. Phys., 10, 11017–11096, doi:10.5194/acp-10-11017-2010, 2010.

Lawrence, M. G., Rasch, P. J., von Kuhlmann, R., Williams, J., Fischer, H., de Reus, M., Lelieveld, J., Crutzen, P. J., Schultz, M., Stier, P., Huntrieser, H., Heland, J., Stohl, A., Forster, C., Elbern, H., Jakobs, H., and Dickerson, R. R.: Global chemical weather forecasts for field campaign planning: predictions and observations of large-scale features during MINOS, CONTRACE, and INDOEX, Atmos. Chem. Phys., 3, 267–289, doi:10.5194/acp-3-267-2003, 2003.

Lelieveld, J., Crutzen, P. J., Ramanathan, V., Andreae, M. O., Brenninkmeijer, C. A. M., Campos, T., Cass, G. R., Dickerson, R. R., Fischer, H., de Gouw, J. A., Hansel, A., Jefferson, A., Kley, D., de Laat, A. T. J., Lal, S., Lawrence, M. G., Lobert, J. M., Mayol-Bracero, O. L., Mitra, A. P., Novakov, T., Oltmans, S. J., Prather, K. A., Reiner, T. A., Rodhe, H., Scheeren, H. A., Sikka, D., and Williams, J.: The Indian Ocean Experiment: Widespread Air Pollution From South and Southeast Asia, Science, 291, 1031–1036, 2001.

Lin, M., Holloway, T., Oki, T., Streets, D. G., and Richter, A.: Multi-scale model analysis of boundary layer ozone over East Asia, Atmos. Chem. Phys., 9, 3277–3301, doi:10.5194/acp-9-3277-2009, 2009.

Logan, J. A.: Tropospheric ozone: Seasonal behavior, trend and anthropogenic influences, J. Geophys. Res., 90, 10463–10482, 1985.

Logan, J.: Trends in the vertical distribution of ozone: an analysis of ozonesonde data, J. Geophys. Res., 99, 25553–25585, 1994.

Marcq, S., Laj, P., Roger, J. C., Villani, P., Sellegri, K., Bonasoni, P., Marinoni, A., Cristofanelli, P., Verza, G. P., and Bergin, M.: Aerosol optical properties and radiative forcing in the high Himalaya based on measurements at the Nepal Climate Observatory-Pyramid site (5079 m a.s.l.), Atmos. Chem. Phys., 10, 5859–5872, doi:10.5194/acp-10-5859-2010, 2010.

Moorthy, K. K., Satheesh, S. K., Babu, S. S., and Saha, A.: Wintertime spatial characteristics of boundary layer aerosols over peninsular India, J. Geophys. Res., 110, D08207, doi:10.1029/2004JD005520, 2005.

Moorthy, K. K., Satheesh, S. K., Babu, S. S. and Dutt, C. B. S.: Integrated Campaign for Aerosols, gases and Radiation Budget (ICARB): An overview, J. Earth Syst. Sci., 117, 243–262, 2008.

Naja, M., Lal, S., Venkataramani, S., Modh, K. S., and Chand, D.: Variabilities in O_3, NO, CO and CH_4 over the Indian Ocean during winter season, Current Sci., 76, 101–107, 1999.

Naja, M. and Lal, S. : Surface ozone and precursor gases at Gadanki (13.5° N, 79.2° E), tropical rural site in India, J. Geophys. Res., 107, doi:10.1029/2001JD000357, 2002.

Naja, M., Chand, D., Sahu, L. and Lal, S.: Trace gases over marine regions around India, Indian J. Mar. Sci., 33, 95–106, 2004.

Naja, M., Lal, S., and Chand, D.: Diurnal and seasonal variabilities in surface ozone at a high altitude site Mt Abu (24.6° N, 72.7° E, 1680 m asl) in India, Atmos. Environ., 37, 4205–4215, 2003.

Nassar, R., Logan, J. A., Worden, H., Megretskaia, I. A., Bowman,K. W., Osterman, G. B., Thompson, A. M., Tarasik, D.W., Austin, S., Claude, H.,Dubey, M. K., Hocking, W. K., Johnson,B. J., Joseph, E., Merrill, J., Morris, G. A., Newchurch, M., Oltmans, S. J., Posny, F., Schmidlin, F. J., Voemel, H., Whiteman, D. N., and Witte, J. C.: Validation of Tropospheric Emission Spectrometer (TES) nadir ozone profiles using ozonesonde measurements, J. Geophys. Res., 113, D15S17, doi:10.1029/2007JD008819, 2008.

Niranjan, K., Sreekanth, V., Madhavan, B. L., and Moorthy, K. K.: Wintertime aerosol characteristics at a north Indian site Kharagpur in the Indo-Gangetic plains located at the outflow region into Bay of Bengal, J. Geophys. Res., 111, D24209, doi:10.1029/2006JD007635, 2006.

Ohara, T., Akimoto, H., Kurokawa, J., Horii, N., Yamaji, K., Yan, X., and Hayasaka, T.: An Asian emission inventory of anthropogenic emission sources for the period 1980–2020, Atmos. Chem. Phys., 7, 4419–4444, doi:10.5194/acp-7-4419-2007, 2007.

Osterman, G., Bowman, K., Eldering, A., Fisher, B., Herman, R., Jacob, D., Jourdain, L., Kuawik, S., Luo, M., Monarrez, R., Paradise, S., Payne, V., Poosti, S., Richards, N., Rider, D., Shephard, D., Vilntotter, F., Worden, H., Worden, J., Yun, H., and Zhang, L.: TES Level 2 Data User Guide, v4.0, JPL D-38042, 20 May 2009, http://tes.jpl.nasa.gov/documents/, 2009.

Park, M., Randel, W. J., Gettelman, A., Massie, S. T., and Jiang, J. H.: Transport above the Asian summer monsoon anticyclone inferred from Aura Microwave Limb Sounder tracers, J. Geophys. Res., 112, D16309, doi: 10.1029/2006JD008294, 2007.

Pfister, G., Pétron, G., Emmons, L. K., Gille, J. C., Edwards, D. P., Lamarque, J.-F., Attie, J.-L., Granier, C., and Novelli, P. C.: Evaluation of CO simulations and the analysis of the CO budget for Europe, J. Geophys. Res., 109, D19304, doi:10.1029/2004JD004691, 2004.

Pochanart, P., Akimoto, H., Kajii, Y., and Sukasem, P.: Regional background ozone and carbon monoxide variations in remote Siberia/East Asia, J. Geophys. Res., 108, 4028, doi:10.1029/2001JD001412, 2003.

Ramachandran, S. and Rajesh, T. A.: Black carbon aerosol mass concentrations over Ahmedabad, an urban location in western India: Comparison with urban sites in Asia, Europe, Canada and the United States, J. Geophys. Res., 112, D06211, doi:10.1029/2006JD007488, 2007.

Ramanathan, V., Crutzen, P. J., Kiehl, J. T., and Rosenfeld, D.: Aerosols, climate and the hydrological cycle, Science, 292, 2119–2124, 2001.

Reddy, R. R., Rama Gopal, K., Reddy, L. S. S., Narasimhulu, K., Kumar, K. R., Ahammed, Y. N., and Reddy, C. V. K.: Measurements of surface ozone at semi-arid site Anantapur (14.62° N, 77.65° E, 331 m asl) in India, J. Atmos. Chem., 59, 47–59, 2008.

Rodgers, C.: Inverse Methods for Atmospheric Sounding: Theory and Practise, World Sci., Hackensack, N. J., 240 pp., 2000.

Roy, S., Beig, G., and Jacob, D.: Seasonal distribution of ozone and its precursors over the tropical Indian region using regional chemistry-transport model, J. Geophys. Res., 113, D21307, doi: 10.1029/2007JD009712, 2008.

Sagar, R., Kumar, B.,Dumka, U. C.,Moorthy, K. K., and Pant, P.: Characteristics of aerosol optical depths over Manora Peak: A high altitude station in the central Himalayas, J. Geophys. Res., 109, D06207, doi:10.1029/2003JD003954, 2004.

Saraf, N.and Beig, G.: Long-term trends in tropospheric ozone over the Indian tropical region, Geophys. Res. Lett., 31, L05101, doi:10.1029/2003GL018516, 2004.

Satheesh, S. K., Moorthy, K. K., Babu, S. S., Vinoj, V., Nair, V. S., Beegum, S. N., Dutt, C. B. S., Alappattu, D. P., and Kunhikrishnan, P. K.: Vertical structure and horizontal gradients of aerosol extinction coefficients over coastal India inferred from airborne lidar measurements during the Integrated Campaign for Aerosol, Gases and Radiation Budget (ICARB) field campaign, J. Geophys. Res., 114, D05204, doi:10.1029/2008JD011033, 2009.

Schell, B., Ackermann, I. J., Hass, H., Binkowski, F. S., and Ebel, A.: Modeling the formation of secondary organic aerosol within a comprehensive air quality model system, J. Geophys. Res., 106, 28275–28293, 2001.

Sheel, V., Lal, S., Richter, A., and Burrows, J. P.: Comparison of satellite observed tropospheric NO_2 over India with model simulations, Atmos. Environ., 44, 3314–3321, 2010.

Shreedharan, C. R.: An Indian electrochemical ozonesonde, J. Phys. E. Sci. Instrum. Sr., 2, 995–997, 1968.

Sillman, S.: The use of NO_y, H_2O_2 and HNO_3 as indicators for ozone-NO_x-hydrocarbon sensitivity in urban locations, J. Geophys. Res., 100, 14175–14188, 1995.

Solberg, S., Hov, Ø, Søvde, A., Isaksen, I. S. A., Coddeville, P., De Backer, H., Forster, C., Orsolini, Y., and Uhse, K.: European surface ozone in extreme summer 2003, J. Geophys. Res., 113, D07307, doi:10.1029/2007JD009098, 2008.

Srivastava, S., Lal, S., Venkataramani, S., Gupta, S., and Acharya, Y. B.: Vertical distribution of ozone in the lower troposphere over the Bay of Bengal and the Arabian Sea during IACRB-2006: Effects of continental outflow, J. Geophys. Res., 116, D13301, doi:10.1029/2010JD015298, 2011.

Steinbacher, M., Zellweger, C., Schwarzenbach, B, Bugmann, S., Buchmann, B., Ordóñez, C., Prevot, A. S. H., and Hueglin, C.: Nitrogen oxide measurements at rural sites in Switzerland: Bias of conventional measurement techniques, J. Geophys. Res., 112, D11307, doi:10.1029/2006JD007971, 2007.

Stehr, J. W., Ball, W. P., Dickerson, R. R., Doddridge, B. G., Piety, C. A., and Johnson, J. E.: Latitudinal gradients in O_3 and CO during INDOEX 1999, J. Geophys. Res., 107, 8015, doi:10.1029/2001JD000446, 2002.

Stockwell, R. W., Kirchner, F., Kuhn, M., and Seefeld, S.: A new mechanism for regional atmospheric chemistry modeling, J. Geophys. Res., 102, 25847–25879, 1997.

Tanimoto, H., Ohara, T., and Uno I.: Asian anthropogenic emissions and decadal trends in springtime tropospheric ozone over Japan: 1998–2007, Geophys. Res. Lett., 36, L23802, doi:10.1029/2009GL041382, 2009.

Tie, X., Madronich, S., Li, G., Ying, Z., Zhang, R., Garcia, A., Lee-Taylor, J., and Liu, Y.: Characterization of chemical oxidants in Mexico City: A regional chemical dynamical model (WRF-CHEM) study, Atmos. Environ., 41, 1989–2008, 2007.

Tie, X., Brasseur, G., and Ying, Z.: Impact of model resolution on chemical ozone formation in Mexico City: application of the WRF-Chem model, Atmos. Chem. Phys., 10, 8983–8995, doi:10.5194/acp-10-8983-2010, 2010.

Uno, I., He, Y., Ohara, T., Yamaji, K., Kurokawa, J.-I., Katayama, M., Wang, Z., Noguchi, K., Hayashida, S., Richter, A., and Burrows, J. P.: Systematic analysis of interannual and seasonal variations of model-simulated tropospheric NO2 in Asia and comparison with GOME-satellite data, Atmos. Chem. Phys., 7, 1671–1681, doi:10.5194/acp-7-1671-2007, 2007.

Venkataraman, C., Habib, G., Kadamba, D., Shrivastava, M., Leon, J.-F., Crouzille, B., Boucher, O., and Streets, D. G.: Emissions from open biomass burning in India: Integrating the inventory approach with high-resolution Moderate Resolution Imaging Spectroradiometer (MODIS) active-fire and land cover data, Global Biogeochem. Cy., 20, GB2013, doi:10.1029/2005GB002547, 2006.

Wang, T. J., Lam, K. S., Xie, M., Wang, X. M., Carmichael, G., and Li, Y. S.: Integrated studies of a photochemical smog episode in Hong Kong and regional transport in the Pearl River Delta of China, Tellus B, 58, 31–40, 2006.

Wiedinmyer, C., Akagi, S. K., Yokelson, R. J., Emmons, L. K., Al-Saadi, J. A., Orlando, J. J., and Soja, A. J.: The Fire INventory from NCAR (FINN): a high resolution global model to estimate the emissions from open burning, Geosci. Model Dev., 4, 625–641, doi:10.5194/gmd-4-625-2011, 2011.

WMO (World Meteorological Organization): Third WMO intercomparison of the ozonesonde used in the Global Ozone Observing System (Canada, 13–24 May, 1991), Global Atmospheric Watch, Rep., 27, Geneva, Switzerland, 1994.

Worden, J., Kulawik, S. S., Shephard, M. W., Clough, S. A., Worden, H., Bowman, K., and Goldman, A.: Predicted errors of Tropospheric Emission Spectrometer nadir retrievals from spectral window selection, J. Geophys. Res., 109, D09308, doi:10.1029/2004JD004522, 2004.

Worden, H. M., Logan, J. A., Worden, J. R., Beer, R., Bowman, K., Clough, S. A., Eldering, A., Fisher, B. M., Gunson, M. R., Herman, R. L., Kulawik, S. S., Lampel, M. C., Luo, M., Megretskaia, I. A., Osterman, G. B., and Shephard, M. W.: Comparison of Tropospheric Emission Spectrometer (TES) ozone profiles to ozonesondes: Methods and Initial Results, J. Geophys. Res., 112, D03309, doi:10.1029/2006JD007258, 2007.

Yu, S., Eder, B., Dennis, R., Chu, S.-H., and Schwartz, S.: On the development of new metrics for the evaluation of air quality models, Atmos. Sci. Lett., 7, 26–34, 2005.

Zhang, M., Uno, I. Zhang, R., Han, Z., Wang, Z., and Pu, Y.: Evaluation of the Models-3 Community Multi-Scale Air Quality (CMAQ) modeling system with observations obtained during the TRACE-P experiment: Comparison of ozone and its related species, Atmos. Environ., 40, 4874–4882, 2006.

Zhang, Q., Streets, D. G., Carmichael, G. R., He, K. B., Huo, H., Kannari, A., Klimont, Z., Park, I. S., Reddy, S., Fu, J. S., Chen, D., Duan, L., Lei, Y., Wang, L. T., and Yao, Z. L.: Asian emissions in 2006 for the NASA INTEX-B mission, Atmos. Chem. Phys., 9, 5131–5153, doi:10.5194/acp-9-5131-2009, 2009.

Zhou, Y., Brunner, D., Boersma, K. F., Dirksen, R., and Wang, P.: An improved tropospheric NO2 retrieval for OMI observations in the vicinity of mountainous terrain, Atmos. Meas. Tech., 2, 401-416, doi:10.5194/amt-2-401-2009, 2009.